

## Exploring the seismic expression of fault zones in 3D seismic volumes



D. Iacopini <sup>a,\*</sup>, R.W.H. Butler <sup>a</sup>, S. Purves <sup>b</sup>, N. McArdle <sup>c</sup>, N. De Freslon <sup>d</sup>

<sup>a</sup> *Geology and Petroleum Geology, School of Geosciences, University of Aberdeen, Meston Building, AB24 FX, UK*

<sup>b</sup> *Euclidity, Santa Cruz de Tenerife, Spain*

<sup>c</sup> *Formerly in JFA, now in Statoil Production (UK) Limited, Aberdeen, UK*

<sup>d</sup> *Impasse Maryse bastie, 44000 Nantes, France*

### ARTICLE INFO

#### Article history:

Received 18 January 2016

Received in revised form

6 May 2016

Accepted 19 May 2016

Available online 27 May 2016

#### Keywords:

Seismic interpretation

Fault structure

Rock deformation

Image processing

Seismic attributes

### ABSTRACT

Mapping and understanding distributed deformation is a major challenge for the structural interpretation of seismic data. However, volumes of seismic signal disturbance with low signal/noise ratio are systematically observed within 3D seismic datasets around fault systems. These seismic disturbance zones (SDZ) are commonly characterized by complex perturbations of the signal and occur at the sub-seismic (10 s m) to seismic scale (100 s m). They may store important information on deformation distributed around those larger scale structures that may be readily interpreted in conventional amplitude displays of seismic data. We introduce a method to detect fault-related disturbance zones and to discriminate between this and other noise sources such as those associated with the seismic acquisition (footprint noise). Two case studies from the Taranaki basin and deep-water Niger delta are presented. These resolve SDZs using tensor and semblance attributes along with conventional seismic mapping. The tensor attribute is more efficient in tracking volumes containing structural displacements while structurally-oriented semblance coherency is commonly disturbed by small waveform variations around the fault throw. We propose a workflow to map and cross-plot seismic waveform signal properties extracted from the seismic disturbance zone as a tool to investigate the seismic signature and explore seismic facies of a SDZ.

© 2016 Elsevier Ltd. All rights reserved.

### 1. Introduction

Many existing interpretations of fault patterns in the subsurface imply relationships between fault geometry, displacement and strain distributed in the surrounding strata. Examples include fold-thrust systems (Boyer and Elliott, 1982; Butler, 1987; Butler and McCaffrey, 2004; Butler and Paton, 2010; Mitra, 1990; Suppe, 1983; Suppe and Medwedeff, 1990; Cardozo et al., 2003; Hardy and Allmendinger, 2011) and normal faults (Cartwright et al., 1995; Cowie and Scholz, 1992; Childs et al., 1996, 2003; Jamieson, 2011; Walsh et al., 2003a,b; Long and Imber, 2010). Fully testing the applicability of these models demands determinations, if not of strain magnitudes then at least descriptions of the strain patterns. The challenge is to map distributed deformation using seismic data. Our aim here is to provide an interpretational framework that could be applied to mapping volumes of deformation in the subsurface using seismic facies concepts that are well-established for high resolution stratigraphic interpretations.

Conventional workflows for seismic interpretation commonly represent faults as discrete planar discontinuities across which stratal reflections are offset (Brown, 1996). Although this approach can greatly facilitate the creation of maps of stratal surfaces and hence the formulation of seismic stratigraphic models, this simplification can hamper understanding of subsurface structural geology (Hesthammer et al., 2001; Dutzer et al., 2009) and impact on the prediction of stratal juxtaposition and consequent models of fluid flow in hydrocarbon reservoirs (e.g. Faulkner et al., 2010). So there is much interest in developing better interpretative tools for seismic data that can predict the structure of complex fault zones, chiefly using seismic attributes (Jones and Knipe, 1996; Chopra and Marfurt, 2005; Cohen et al., 2006; Gao, 2003, 2007; Iacopini and Butler, 2011; Iacopini et al., 2012; McArdle et al., 2014; Botter et al., 2014; Hale, 2013 for a review; Marfurt and Alves, 2015). This contribution develops this theme further. We focus on two examples, one a normal fault zone (Taranaki Basin, New Zealand) and another a thrust zone (deep-water Niger Delta), using single and combined seismic attributes. Although these approaches are widely used to predict stratigraphic geometries in the subsurface,

\* Corresponding author.

E-mail address: [d.iacopini@abdn.ac.uk](mailto:d.iacopini@abdn.ac.uk) (D. Iacopini).

they have hitherto seen little application to the structural interpretation of seismic data. Therefore we outline the geophysical basis for the methods here – with greater detail reserved for the appendix.

Some of the issues affecting structural interpretation of faults are exemplified in Fig. 1. While some parts of the data appear to show discrete offsets across narrow zones where seismic amplitude is greatly reduced, other levels show broader areas of amplitude reduction. This could represent zones of more broadly dispersed deformation, such as are found in fault relays (Childs et al., 1996, 2003; Walsh et al., 1991, 2002, 2003a,b). An indication of these broader deformation zones is manifest here as the folding of stratal reflectors both in the hangingwall and footwall to the fault zone.

To further guide our studies, we refer to outcrop analogues for deformation structures developed in sandstone-shale multilayers (Fig. 2). In these small-scale situations, the deformation is very rarely focused onto a single fault surface. Although a single sub-planar discontinuity can commonly be identified upon which much of the displacement has been accommodated, this principal structure generally has other deformation surrounding it. For the thrust structure shown here (Fig. 2a), deformation includes folding, so that strata are locally sub-vertical, and include deformation fabrics (weak cleavage) and secondary faults. In the case of the fault example (Fig. 2b), although the bedding are gently folded, arrays of secondary faults with variable dipping orientation (Fig. 2c) create offsets of strata on various scales. In both cases the deformation away from their respective principal faults disrupts bedding. Consequently we infer that if these examples are representative, suitably up-scaled, for those in the subsurface, these secondary structural features should be manifest in seismic data. The challenge is to identify and interpret these – at least to isolate stratal

volumes where these secondary deformations are most concentrated. This is the central aim of our paper.

## 2. Methodology

### 2.1. Seismic attributes

Attributes are measurements based on seismic data such as polarity, phase, frequency, or velocity (Dorn, 1998). They are calculated through signal and image processing algorithms and are used for both qualitative and quantitative interpretation of seismic dataset. Our approach uses seismic attributes to provide information carried by the seismic signal that is otherwise not used in conventional seismic mapping. When interpreting stratigraphic features such as channels and marginal units to carbonate reefs (Marfurt and Chopra, 2007), different attributes are combined to create so-called “seismic texture” maps. The term “seismic texture analysis” was first introduced by Haralick et al. (1973). Love and Simaan (1984) subsequently applied the concept to extract patterns of common seismic signal character. The approach gained favor because sedimentary features with common signal character could be related to their inferred depositional environment (Fournier and Derain, 1995). Subsequently a plethora of seismic attributes and textures have been developed - using statistical measures to quantify stratigraphic interpretations by creating repeatable seismic facies to predict subsurface reservoir characteristics (Gerard and Buhrig, 1990; Evans et al., 1992; Gao, 2003, 2007; Schlaf et al., 2004; Chopra and Marfurt, 2005; West et al., 2002; Corradi et al., 2009). The 1990s saw 3D attribute extractions become commonplace in the interpretation work place. During this time seismic interpreters were making use of dip and

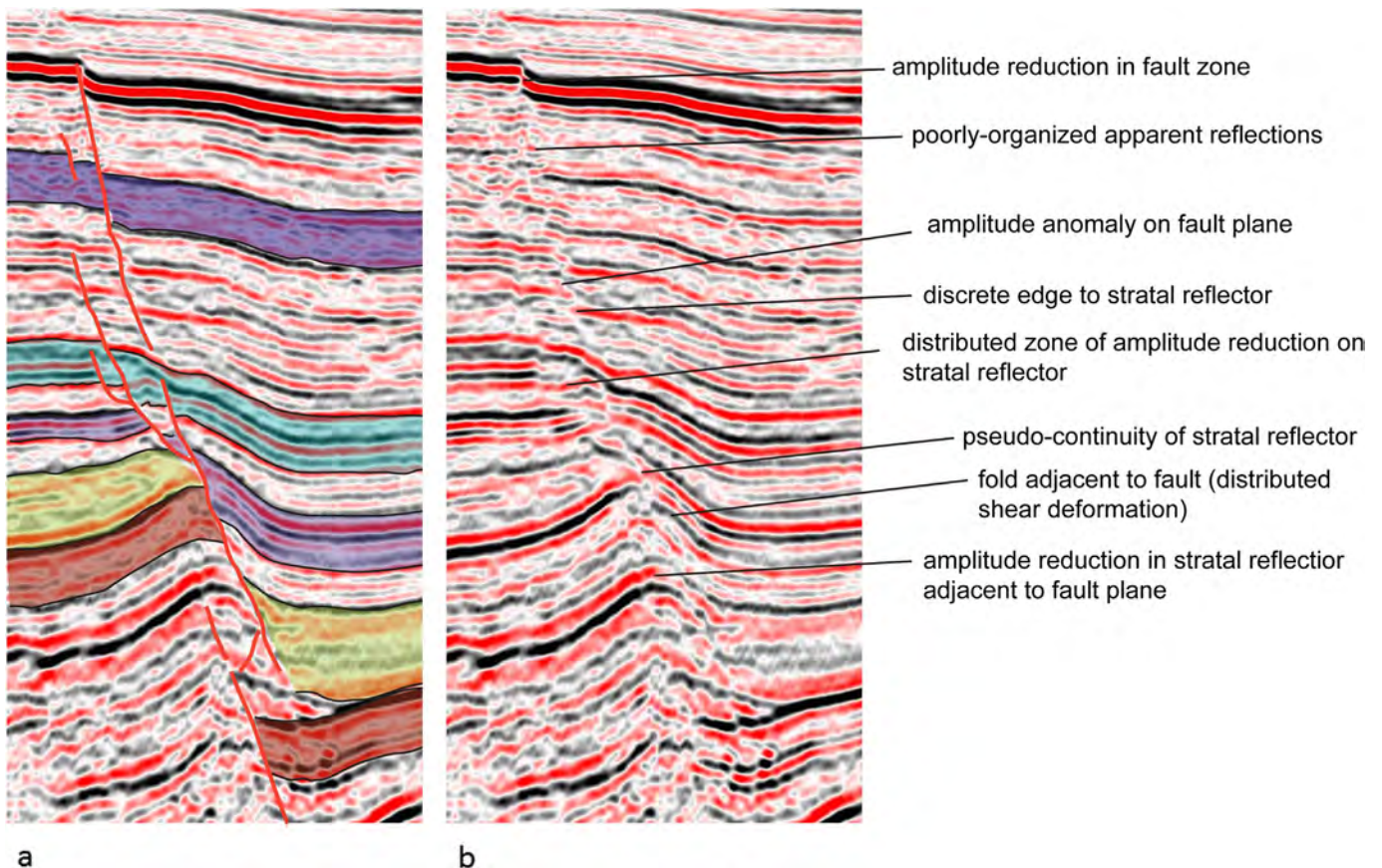
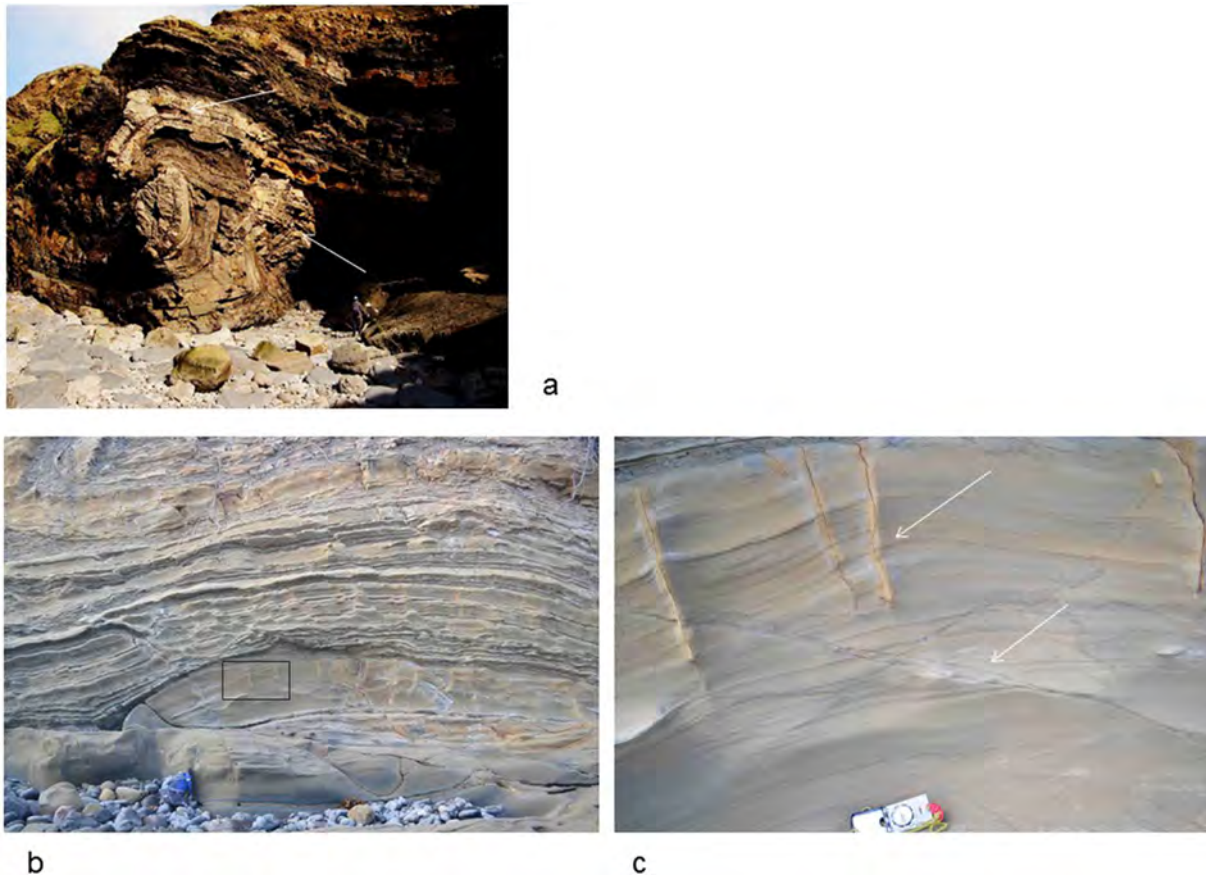


Fig. 1. a) Interpreted seismic image of a normal fault structure and related damage (North sea, Virtual SA library). b) Characterization of the main reflectors along the fault structure.



**Fig. 2.** a) View of a classical thrust structure, Prembokshire (UK). Arrows pointing respectively at the thrust fault and related anticline. b) thrust fault on turbidite complex, Army bay, New Zealand; c) zoomed view of b (black rectangle), on the small scale damage and fracture.

azimuth maps (Brown, 1996). Amplitude extractions and seismic sequence attribute mapping were also established (Chopra and Marfurt, 2007). In order to reveal subtle stratigraphic features (e.g. buried deltas, river channels, reefs and dewatering structures), datasets were pre conditioned (e.g. filtering random noise and pre calculation of large scale linear or anisotropy features) leading to cross-correlation and coherence analysis (Marfurt and Chopra, 2007). Further, dataset processing that preserved seismic amplitude has subsequently been used to infer porosity, statal thicknesses and lithology. Computations of curvature on amplitude, envelope or impedance have proven efficient in describing structural or channel lineament (Chopra and Marfurt, 2007, 2010). Here we describe an equivalent single and multi-attributes analysis on pre-conditioned seismic datasets in order to characterize styles of seismic response around selected larger scale deformation structures that can otherwise be mapped conventionally using standard amplitude displays.

## 2.2. Noise analysis

Subsurface discontinuities create reflections and diffractions in seismic reflection data (Khaidukov et al., 2004). Reflections are used conventionally to interpret structural and stratigraphic features as they are generated by interfaces with impedance contrasts. Diffractions are generated by local discontinuities that act like point-sources (Neidell and Taner, 1971; Zavalishin, 2000), becoming active as soon as the direct wave hits them. Commonly, if those points are of the size comparable to the seismic wavelength (the Rayleigh criterion), they are ignored during processing

(Khaidukov et al., 2004). Consequently this imposes a limit on the resolution of recorded backscattered waves: below the Rayleigh limit (Moser and Howard, 2008; Gelius and Asgedom, 2011) no definite answers can be given as to location, dip, and curvature of a discontinuity, nor its topological properties, such as connectivity. An example of these limits is illustrated in Fig. 3a, part of a dip line extracted from a stacked 3D seismic volume. Here a discontinuity, inferred to represent a thrust fault, is surrounded by a halo characterized by low amplitude and incoherent seismic traces (the square box b Fig. 3a, b). The same characteristics are retained even after smoothing (Fig. 3c). This part of the seismic volume represents a width of several 10–100 m (see Fig. 3c for scale), which is significantly larger than the Rayleigh limit of resolution. Therefore this volume should contain primary reflections. That these are obscure suggests that the volume contains disruptive geological structures – potentially deformation equivalent to that associated with outcropping faults (e.g. Fig. 2b). Dutzer et al. (2009) called these “seismic fault distortion zones”: volumes within the seismic data of significant uncertainty where the signal is distorted. Iacopini and Butler (2011) termed these volumes of disrupted seismic signal “disturbance geobodies”, where geobodies are interpreted 3-D objects that contain voxels with similar seismic amplitudes or other seismic attributes. Some disturbance geobodies, or components thereof, may relate to imaging problems (sensu Fagin, 1996), such as migration issues or/and interference by diffractions due to the geometrical complication of strata and edges around the faults and folds. Others however may indeed represent deformation. Here we focus on the seismic properties and internal geometry of disturbance geobodies by analysing the performance

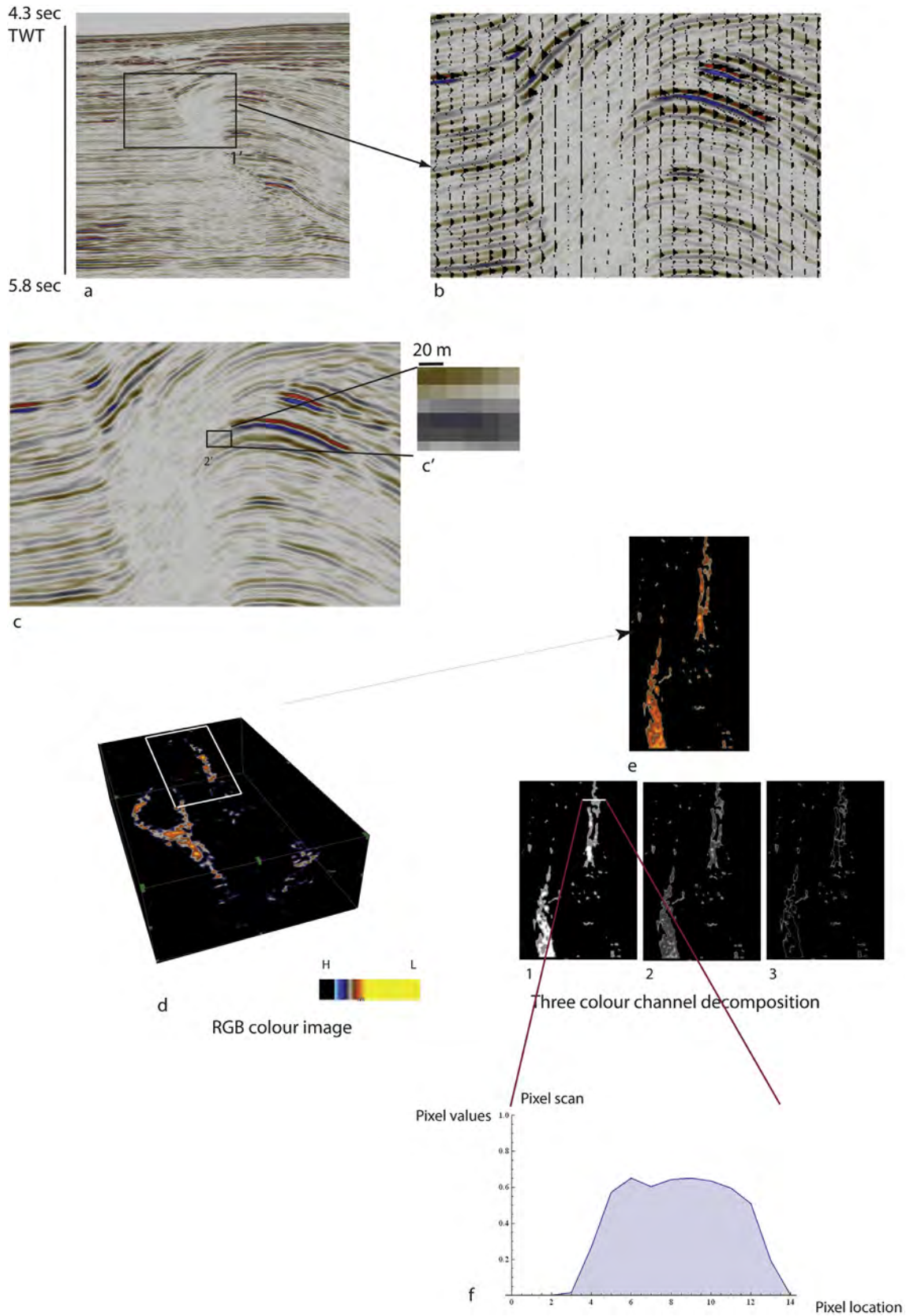


**Fig. 3.** Images of a seismic disturbance zone (SDZ): a) original thrust structure (Niger delta); b) wiggled visualization of the magnified view from the main stacked trace in box 1'; c) smoothed visualization of the stacked image b; c') voxel visualization and scale of box 2'; d) Geobodies representing the SDZ of a thrust extracted from a 3D volume (black colour, (high coherency) put in transparency). e) RGB time slice colour imaging the SDZ cross thrust strand in d; 1. the correspondent red channel (RGB) expressed through the grey scale channel (preserving the internal colour gradient), 2: second green channel (RGB); 3 third (correspondent blue) channel expressing the edge component of the RGB; f) plot diagram of the pixel values scan analysis across the first channel bright monochrome SDZ image. (For interpretation of the references to colour in this figure legend, the reader is referred to the web version of this article.)

of filters and filter sequences that can be applied during an image-processing workflow, especially those that inform interpretation of the distribution of the seismic noise within post stack seismic datasets. We then introduce some simple cross-plotting techniques so as to investigate the correlation between main phase and coherence attributes and to define possible seismic facies within geobodies. We believe that this approach can extend the use of seismic data in extracting more geological information (at scales above the Rayleigh limit) to interpret signal distortions associated with larger-scale deformation structures.

### 2.3. Image processing techniques

Digital images, representing the seismic waveform, can be sampled and converted to discrete valued integer numbers through a process of image quantization (Acharya and Ray, 2005). The smallest single sampled component of a digital image is a voxel. Any image is therefore subdivided into voxels (Fig. 3c') and voxel coordinates are indexed as a matrix of rows and columns. In seismic image processing each voxel is associated with an intensity of the colour that is proportional to the value of a particular attribute (Acharya and Ray, 2005 and Fig. 3f). The number of bits used to represent the value of each voxel determines how many colours or shades of grey can be displayed and as a consequence how much detail we can expect to track in the signal analysis (Henderson et al., 2007, 2008). As an example see an image excerpt representing a geobody (Fig. 3d) that has been sliced (Fig. 3e) and decomposed across three channels (1,2 and 3 in Fig. 3e) and then scanned through. The single colour brightness is associated with voxel values and can be easily extracted for further quantitative analysis.

Using processed images we can describe structurally-oriented disturbed and low signal-to-noise zones surrounding faults and other deformed zones. Post-stack seismic data are used here. We aim to demonstrate that such disturbed zones can be analyzed using different coherency algorithms and cross-plotted through 3D image visualization and image processing tools. The image techniques and workflow proposed here can readily be represented and reproduced through a variety of image processing codes and commercial/open source software (see also appendix).

### 3. The fault seismic disturbance zones (SDZ)

Conventional interpretation workflows pick faults from offset stratal reflectors on seismic data to create discrete, sub-planar surfaces (Fig. 4a). While this approach certainly tracks the discontinuity and highlight the main fault relative displacement, it overlooks any deformation structures surrounding the simple edge discontinuity (Fig. 4b). Signal disturbance can also be found in 3D seismic volumes that are related to folds (Fig. 4c, d). In these cases the volumes of signal disturbance, while characterized by chaotic and discontinuous reflector geometry, retain some amplitude and phase properties (see examples in Fig. 4d, e). We term these *Seismic Disturbance Zones (SDZs)* and they may have several distinct explanations: inappropriate illumination during the acquisition (Vermeer, 2009); the incorporation of diffractive components during the stacking procedure (Neidell and Taner, 1971); and an inappropriately-simplified velocity model within the deformed area (Zhang and Sun, 2009; Biondi, 2006). All will contribute to the blurring of the signal by down-grading the signal/noise ratio in faulted, damaged and folded volumes. The lower physical limit of any interpretation is constrained by the ray tracing assumption, which is defined by the vertical tuning thickness (frequency), that is approximately one quarter of the seismic wavelength (see Widess, 1973; Partyka et al., 1999), and laterally by the dimensions of the Fresnel zone that, for depth-migrated seismic, is of the order of the

wavelength (Berkhout, 1984). So there is a scale, between the Rayleigh limit and the distinctive seismic response, where signal expression is strongly disturbed but can still be interpreted. Our challenge is to use information from SDZs to enhance interpretations of distributed deformation around faults. The question here is: to what extent we can push our interpretation using signal and image analysis methods? To answer this we now analyse two different examples.

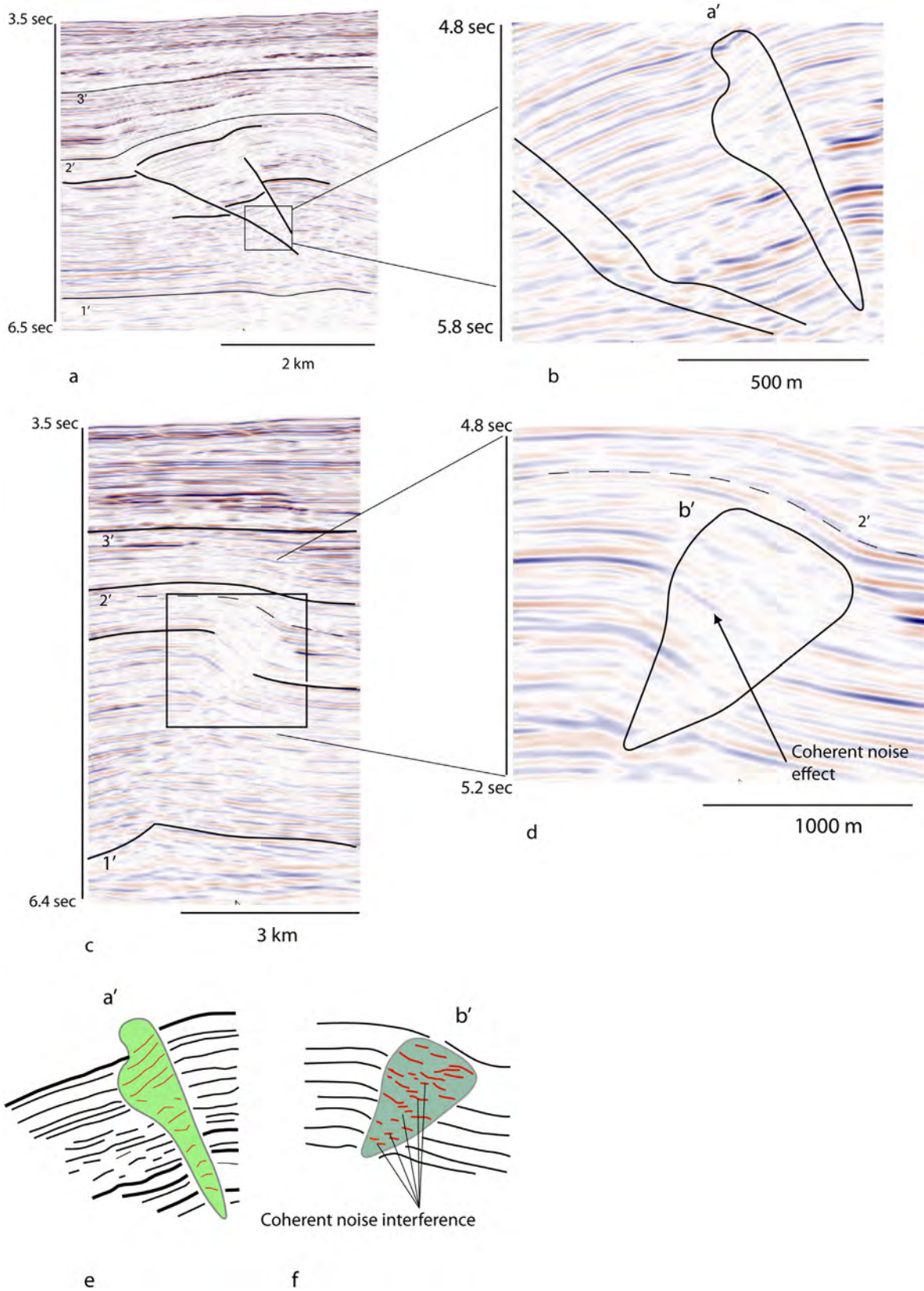
### 4. Expression and internal architecture of SDZ of a normal fault

Fig. 5 illustrates a section of the Parihaka normal fault located along the western margin of the Taranaki Basin offshore New Zealand (Fig. 5a, Giba et al., 2010). The example (Fig. 5a') is located along the western margin of the Taranaki Basin offshore New Zealand. Growth strata indicate that the Parihaka Fault accrued displacement during Late Cretaceous-Early Eocene extension (Fig. 6a) and was reactivated during renewed extension s affecting Early Pliocene strata (ca 3.7 Ma). A detailed analysis of this structure is provided by Giba et al. (2010, 2012).

Cursory examination of the seismic data reveals discrete stratal offsets across a narrow tract with low signal/noise character (Fig. 6a), presumably representing the main fault strands. However, these faults are encased, both in the hangingwall and footwall, by seismic volumes within which the continuity of stratal reflectors is disrupted and small-scale offsets of reflectors are evident (Fig. 6b). We infer that these zones of signal disruption represent locally-intense small to medium scale structural damage (Fig. 6c), collectively representing a SDZ 1–3 km wide.

#### 4.1. Internal expression of the SDZ

The challenge now is to investigate the internal character of the SDZs. Various approach has been proposed so far in to image processing literature. Hu et al. (2010) proposes a de-blurring filter, while Fehmers and Höcker (2003) developed a Structural Oriented (SO) filter to track similar discontinuities. Fehmers and Höcker (2003) and Hale (2013) then further apply the SO filter within semblance algorithm (calling it SO semblance) to estimate fault throws. The SO semblance attribute is generally calculated by identifying the orientation of maximum semblance and outputting the value associated with that orientation. It automatically looks at all orientations around each point in the data to find the correct structural orientation. This may require a certain pre-conditioning of the dataset through the calculation of dip and azimuth steering volumes (Gersztenkorn and Marfurt, 1999). The SO semblance attribute is independent of amplitude and heavily influenced by phase, so it readily identifies phase breaks in the data irrespective of the amplitude. A similar approach is the Tensor coherency (or eigen-structure coherency; see Gersztenkorn and Marfurt, 1999) which represents an analytical method calculated through combination of the eigenvalues of the gradient structure tensor for the data of interest. The tensor attribute is very sensitive to amplitude changes in the data (high amplitude data has a larger gradient change across a fault than low amplitude data) and therefore tends to be more resistant to “noise” that can appear in coherency attributes from low amplitude chaotic strata. More sophisticated image-processing workflows targeting the fault damage using a combination of structurally-oriented filters and seismic attributes have recently been proposed (Duzter et al., 2009; Iacopini et al., 2012; Hale, 2013). The combined use of the tensor attribute and S–O semblance has the potential to distinguish the displacement zones from broad tracts of general signal disturbance (Iacopini and Butler, 2011; Iacopini et al., 2012). Specifically in this paper we have



**Fig. 4.** Seismic line representing a 2D section from deep water thrust of the Niger Delta. b) Zoomed view of the boxed area in Fig. 4a representing delimited SDZ zones characterized by area of low amplitude and disturbed signal. c) Seismic line representing a section 500 m apart along strike from the image in a showing a backfold limb structure. d) Zoomed image from the square box area in c) showing the low amplitude and SDZ area. Arrow pointing to a footprint oriented noise affecting the SDZ. e) Sketches of the upper thrust SDZ imaged in e b; f) sketch of the backlimb SDZ imaged in d).

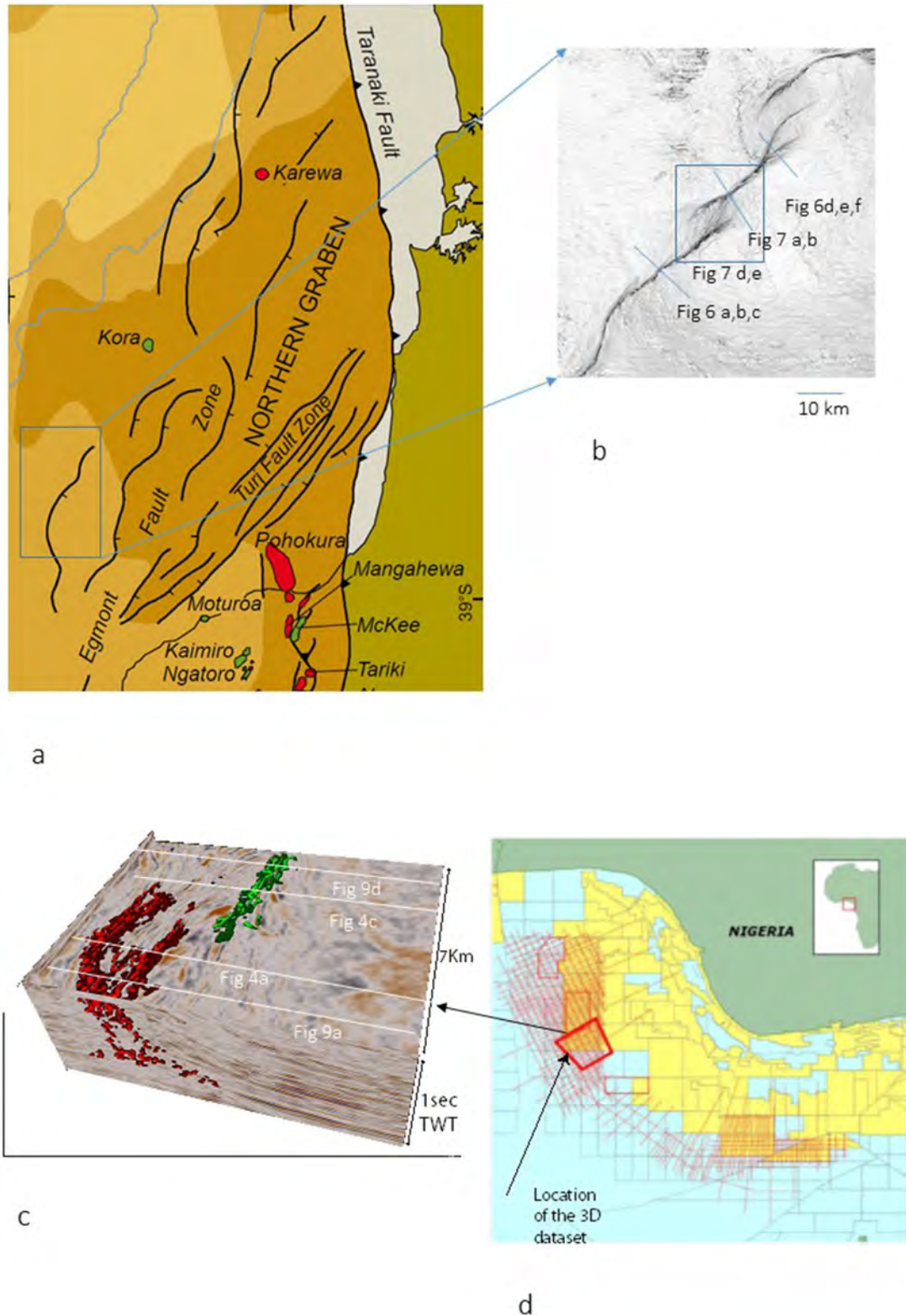


**Fig. 5.** a) Regional location of the Parihaka fault (modified from the New Zealand Ministry of Petroleum and Minerals regional map). b) Time slice semblance coherency visualization (at 900 ms TWT, within the upper Pleistocene) of the Parihaka fault. Section lines show the location of the seismic sections in Figs. 6 and 7. Rectangle shows time slices in Figs. 7d, e and 10. c) 3D visualization of the deepwater Niger delta thrust structure. The grey section traces represents the seismic image proposed in Figs. 4a, c and 9a, d. d) Location of the deep water thrust system discussed and represented in Fig. 4c.

adopted a modified version of the main workflow procedure described in Iacopini et al. (2012) and briefly highlighted in the Appendix. Taner et al. (1979) and Purves (2014) describe and

discuss the underlying physics associated with complex attributes such as instantaneous phase.

In order to express the seismic texture of the main internal

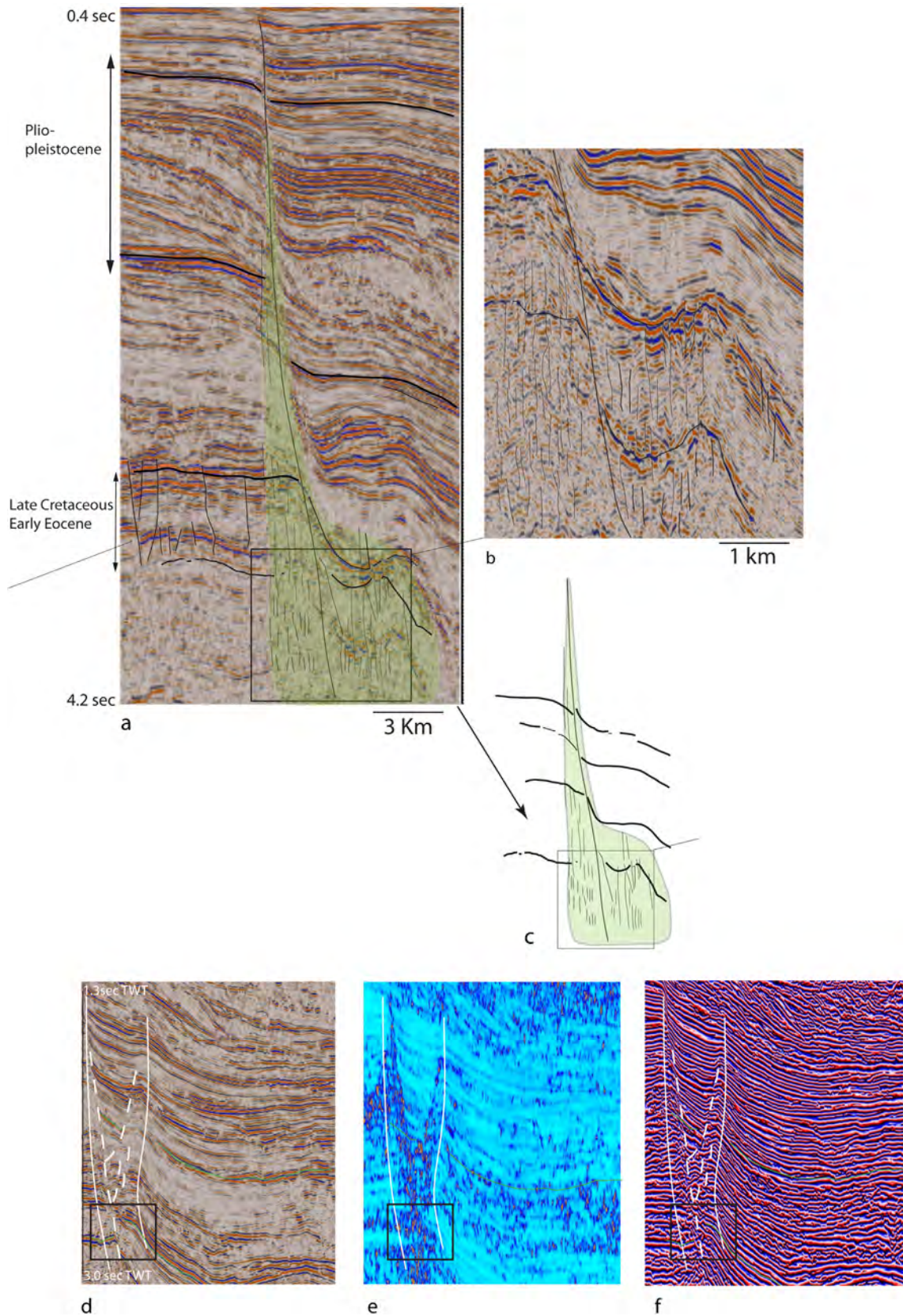


**Fig. 6.** Seismic sections in amplitude of: a) Parihaka normal fault (see Fig. 5b for location); b) zooming of the SDZ across the main fault structures; c) simplified sketch of the lower main damage zones in c. Seismic section from the Parihaka fault (d to f, location in Fig. 5b) imaged through various attributes d) fault image in amplitude; e) semblance coherency; f) instantaneous phase. White dotted lines map the major discontinuities with visible displacement across the SDZ zone. Continuous white lines define the boundaries of the SDZ.



structure of the SDZ, in our interpretation we analyse and compare the amplitude, SO semblance coherency and the instantaneous phase expression of the signal. First we apply these three attributes to a segment of the fault (Fig. 5) and discuss their capabilities in enhancing different seismic aspects of the SDZ.

#### 4.1.1. Amplitude expression

The fault zone in Fig. 6d is surrounded by a SDZ of small-scale faults that affect the continuity and coherency of the amplitude signal. The SDZ includes not only the fault core zone (where the displacement is localized, as indicated by the white dotted lines) but also variable portions of the boundary walls where the signal is strongly disturbed. This distributed zone varies in width between 50 and 200 m.

#### 4.1.2. SO semblance coherency

A semblance coherency image is represented in Fig. 6e. The colour scale is set such that bright yellows represent low semblance values (strong variability of waveform properties across the traces) while blue colours represent high semblance coherency areas. Incoherency is found not only associated with the main discontinuities but also within the adjacent SDZ (bold white line) where it shows similar scattered low values of coherency. Using opacity controls, semblance can also track the main discontinuities in the stratal reflectors together with amplitude variations along these reflectors.

#### 4.1.3. Instantaneous phase

Instantaneous phase (the phase component of the Hilbert transformation of the seismic dataset; [Taner et al., 1979](#), [Purves, 2014](#)) is effective at highlighting phase-dependent properties such as thin bed-sets, reflection terminations and other discontinuities in stratal reflectors. This attribute is commonly used to enhance interpretations of discontinuous stratal patterns such as onlap and offlap ([Chopra and Marfurt, 2007](#)). Within the SDZ (Fig. 6f), reflectors are characterized by discontinuities and/or chaotic structures. The instantaneous phase attribute reveals sub-structure within SDZs that, using semblance, are not otherwise imaged.

In the specific case studied here, the comparison of the images using three different expressions (amplitude, semblance and instantaneous phase) indicates that small scale faults are tracked and registered by coherency attributes and stratigraphically unraveled by phase-related attributes. It is through the combined use of these various attributes that structural interpretation of the faults is enhanced.

## 4.2. Image analysis of the tensor and SO semblance

Our objective now is to understand if displacement features currently mapped by the semblance attribute can be distinguished from disturbance zones associated with reflector disruption or edge reflectors. Edge reflectors produce clear lateral de-phasing of the signal between traces and can track discontinuities down to the limit of the tuning thickness. To explore these signal responses we use the tensor attribute and the Structural Oriented semblance attribute (SO semblance) as illustrated in a seismic inline across the Parihaka fault (Fig. 7a–c, for location see Fig. 5b). Low coherency zones tracked by the tensor attribute are draped on the original amplitude section (now as a semi-transparent image; Fig. 7b). SO semblance attributes are calculated and draped on the original amplitude section (as transparent image; Fig. 7c). The tensor attribute highlights the main discontinuities related to the edge reflector termination and the incoherent zones (Fig. 7b) with minimal response along the continuous reflectors or in the low

amplitude zones. In contrast, the SO semblance attribute highlights a number of small scale discontinuities in the low amplitude zone that correspond to phase breaks due to chaotic or partially resolved reflectors (Fig. 7c). A similar comparison between attributes can be made using a time-slice (Fig. 7d,e; for location see Fig. 5b). The tensor attribute (Fig. 7e) also tracks the main faults and highlights them with better contrast than the semblance coherency (Fig. 7d).

Comparison between the two attribute approaches can also be made for specific stratal horizons. Here we visualize a stratal reflector for a horizon mapped within the late Pliocene units and crossing a relay ramp on the main Parihaka fault. The edge of the fault is imaged by the tensor coherency (Fig. 8a). The same horizon is then analyzed through the SO semblance coherence (Fig. 8b). This attribute also tracks edges and thus identifies the main fault discontinuity, but it is also very sensitive to other sources of incoherency surrounding the main fault throw. These surrounding areas broadly correspond to zones of strong amplitude variability here expressed as envelope of the amplitude (Fig. 8c) although a clear linear relationship between amplitude and semblance coherency values is not evident (Fig. 8d). Some of these incoherency sources may relate to the design of the original seismic acquisition (in relation to the structure) and to stratigraphic heterogeneities such as small sedimentary bodies and channels. However, the concentration of incoherency in the vicinity of the fault relay ramp (Fig. 7b) may suggest that the attribute is also detecting stratal layers that contain higher concentrations of minor deformation structures.

Using the two coherence attributes in tandem (Fig. 8a, b) not only enhances the image of the main fault zone, it also permits detection of smaller scale deformation in the surrounding strata. Thus not only can maps of fault throw and other products used for fault analysis be enhanced, seismic data can also be used to test kinematic models for the deformation state of fault wall rocks that are derived from the larger-scale displacement fields (e.g. [Wibberley et al., 2008](#); [Faulkner et al., 2010](#)).

## 5. Expression and internal architecture of SDZ of a thrust fault

To demonstrate the broader utility of the workflows outlined above, we now address a contractional structure, imaged from 3D seismic data from the deep water Niger delta fold and thrust Belt, analyzed and presented here in TWT (two way travel time). This structure is introduced by [Higgins et al. \(2007, 2009\)](#). Further structural context is provided by [Iacopini and Butler \(2011\)](#). Consider two profiles, 500 m apart along strike (Fig. 4a, c). Both show a basal detachment (1'), a sequence of pre-kinematic strata (2'), a sequence of syn-kinematic strata (with respect to the local structure; 3') and post-kinematic strata (3' up to the seabed). These strata are all part of the Agbada Formation, a succession of turbidite sandstones, shales and associated debrites. The detachment zone is focussed in the largely over-pressured Akata shale ([Higgins, 2008](#)).

In one profile the pre-tectonic package is deformed by an opposed pair of thrust faults that deflect and offset the stratal reflectors (Fig. 4a). In contrast, the adjacent section (Fig. 4c) shows a fold structure. The main discontinuities and fold have uplifted the top of the pre-kinematic strata by 1–2 km above their regional elevation, assuming mean seismic velocity ranges from 3 to 3.5 km/s ([Morgan, 2003](#)). The double-thrust structure is not defined by discrete zones of offset. Rather it is marked by a volume within which the seismic signal is disrupted (4.8 s and 5.8 s TWT on Fig. 4b). These volumes are about 100 m wide. Reflectors entering these volumes become chaotic, blurred and reduced in amplitude. This represents a fault-associated SDZ. A magnified view of the fold structure (Fig. 4d) illustrates broader tracts of signal disturbance.

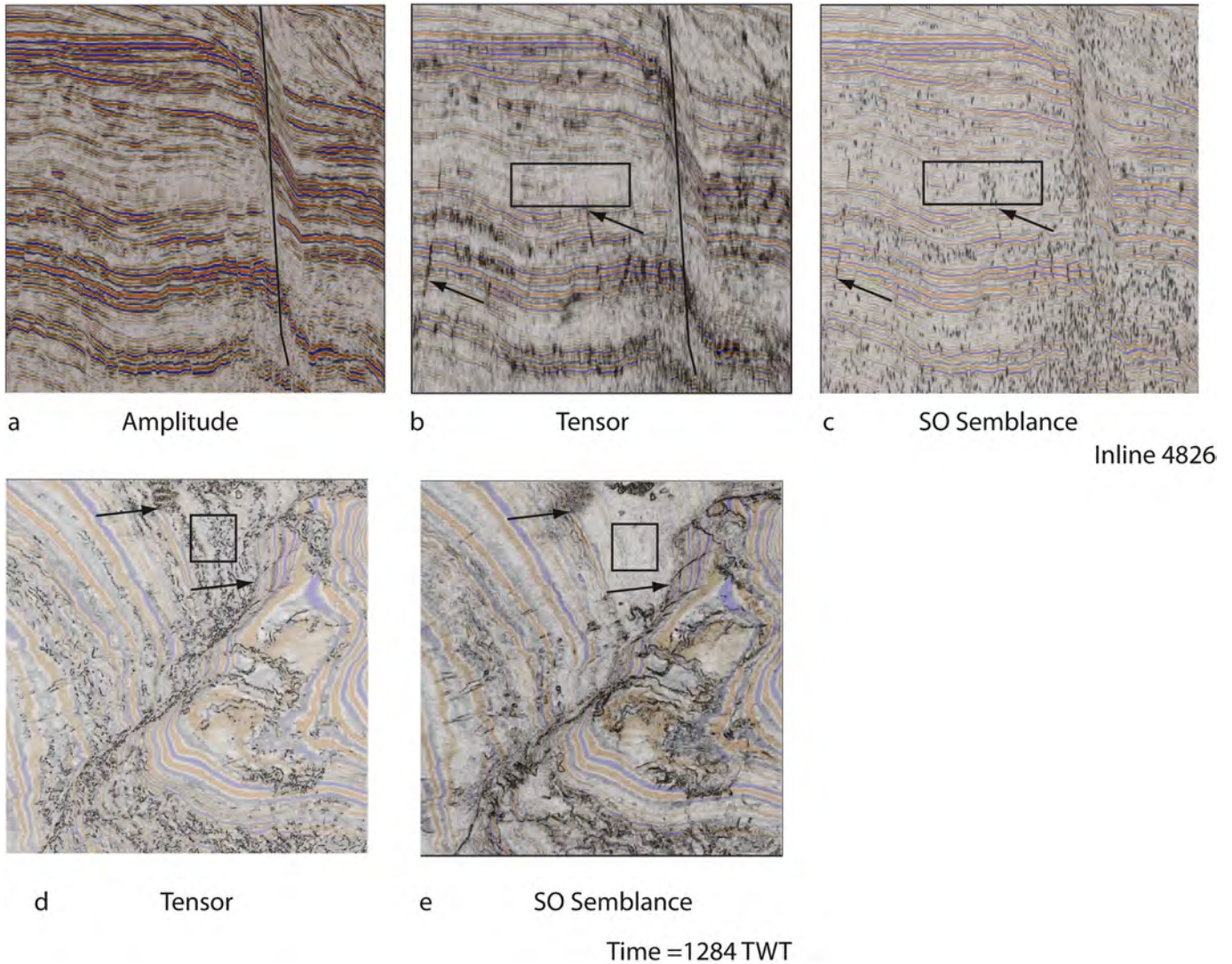


**Fig. 7.** Comparison of the tensor coherency and the SO semblance coherency filters across the main Parihaka fault. a) Seismic section amplitude image; b) tensor attributes expression draped on the original image a) (now in transparency); c) semblance attributes draped on the amplitude image a) (now in transparency: the amplitude image). d) Tensor attributes draped on the time slice amplitude image from the Parihaka fault; e) SO semblance coherency attributes draped on the time slice amplitude image (at 1284 ms TWT). See further explanation in the text. Arrows and boxes are used for comparisons. Location of seismic section and time slice is shown in Fig. 6b.

Part of the signal expression here is characterized by coherent dipping noise interfering with the continuous reflectors (arrow in Fig. 4d). This tract can be mapped and the SDZ contoured (Fig. 4d) to delimit and extract geobodies with low signal to noise ratios. We can then use these geobodies to provide more realistic descriptions of thrust zones and associated deformation. These SDZs and their associated geobodies have length of kms along strike and thicknesses of 50–100 m (Fig. 4b) to 500 m and therefore represent significant volumes of deformed strata.

### 5.1. Internal expression of the SDZs

#### 5.1.1. Amplitude expression

In Fig. 9a (few km apart from Fig. 4a) the main discontinuity (expressed in amplitude) is interpreted to be a large-scale thrust fault that deflects the lower part of the Agbada Formation. It terminates upwards into a triangular zone of signal disturbance where the amplitude is strongly damaged reduced. There is also significant amplitude-dimming and signal disturbance around the thrust zone itself. This behaviour can be tracked along strike to an

adjacent section (Fig. 9d). Here there is a similar amplitude reduction in the core of the fold. The details of the image suggest that the dislocation of stratal reflectors is chiefly confined to the deeper part of the SDZ, near the fault nucleation zones, while the upper part rather defines a broadening low Signal/Noise (S/N) zone while still preserving the continuity of the main folded stratal reflectors.

#### 5.1.2. SO semblance coherency

The disturbance zone surrounding the thrust-cored anticline (forelimb) is mapped as a strongly incoherent tract (Fig. 9b), with the greatest incoherency associated with the core of the structure. The backlimb of the anticline also contains small inclined zones of incoherency (with similar relative values as thrust core; Fig. 9f). Specifically in Fig. 9f the semblance coherency in the backlimb closely corresponds to the change in dip (kink) of the reflectors. These do not align along a single axial plane, but show a more complex geometry. The low coherency zones do not correspond to significant offsets of the stratal reflectors (as confirmed by the amplitude and phase image Fig. 9a,d and c,f). The images support

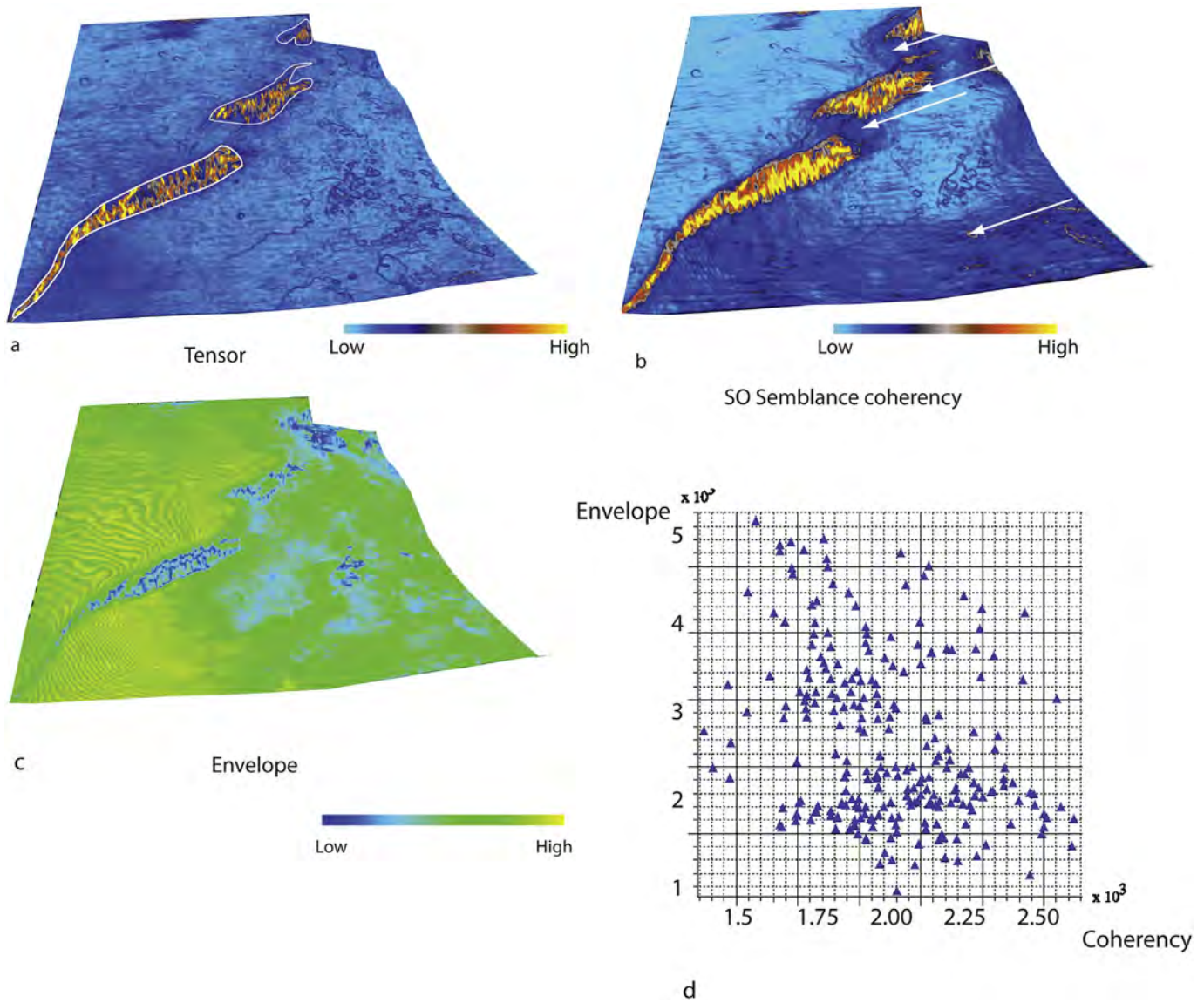


**Fig. 8.** 3D imaging of a shallow horizon crossing the parihaaka fault showing: a) the tensor coherence across the parihaaka fault structure. b) the SO semblance coherence across the Parihaka fault structure. c) the envelope distribution across the Parihaka fault structure. d) cross-plot representation of the envelop versus coherency values extracted from the fault through.

the conclusion of [Iacopini and Butler \(2011\)](#) that semblance coherence may be used to identify stratal volumes containing distributed deformation rather than be used to simply detect edges (e.g. fault-cutoffs) of stratal reflectors.

### 5.1.3. Instantaneous phase

The internal structures tracked by the semblance coherence attribute are better imaged visually using the instantaneous phase, especially the thin-bed discontinuities and reflector breakages. [Fig. 9c](#) shows that discrete offsets and breaks of the stratal reflectors are confined to the lower medium part of the structure. Likewise instantaneous phase does not image breaks in stratal reflectors but rather their bending along the axial plane of the anticline ([Fig. 9f](#)). Both profiles resolve well the stratigraphic contact between the Agbada and Akata Formations (green lines, [Fig. 9a, d](#)) and show that it has been offset by the large-scale thrust (>5.2 s TWT).

Combining the two seismic attributes (semblance coherence and instantaneous phase) improves the imaging and helps to

elucidate the nature of the large scale SDZ. Semblance coherence can be applied to recognize an area of possible deformation associated to seismic waveform incoherency. Following this initial analysis, instantaneous phase can be then be applied to fine-tune definition of the principal fault discontinuities, and thus establish lateral stratal continuity within individual SDZs.

## 6. Cross-plot analysis

In earlier contributions we have attempted to delimit SDZs and investigate their internal seismic structure ([Iacopini and Butler, 2011](#); [Iacopini et al., 2012](#)). We also applied the cross-plot analysis by comparing the semblance and the curvature to enhance and characterize zones affected by different strain ([Iacopini and Butler, 2011](#)). A similar combined approach was also proposed by [Chopra et al. \(2011\)](#) to characterize horst and graben structures. We did not however address how to distinguish (in a stacked seismic dataset) the signal components deriving from the oriented

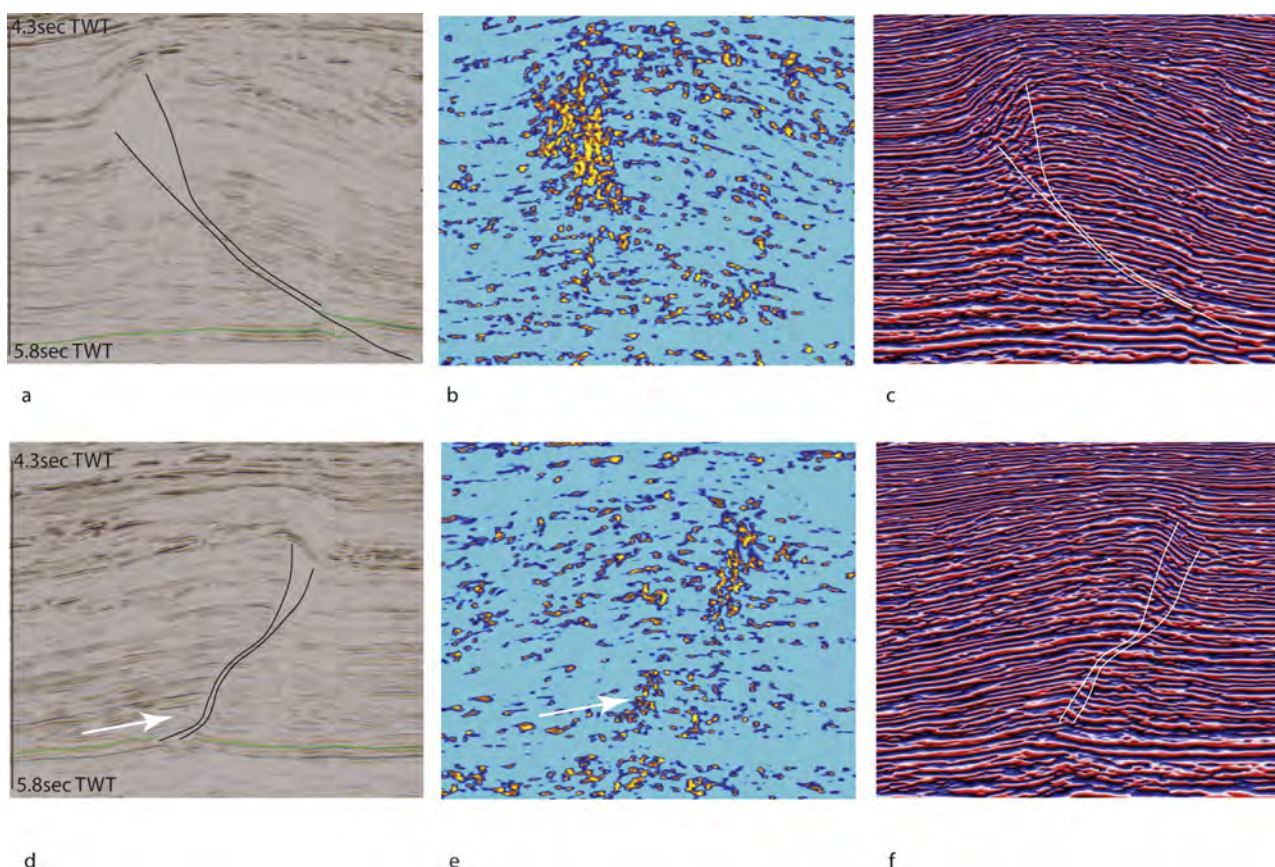


**Fig. 9.** Two seismic sections from the deep water Niger Delta FTB imaged through different attributes: a) foredeep thrust image in amplitude; b) semblance/coherency image from a; c) instantaneous phase image from a; d) image in amplitude of a section 1 km apart from a showing a backfold structure; e) semblance/coherency image from d; f) instantaneous phase image from d.

structure from noise, be it arising from the background or created by surrounding structures. This enhancement is now discussed with reference to pre-conditioning the seismic data through simple cross-plotting methods. The approach is then applied to our two case studies.

### 6.1. Rationale of cross-plotting seismic attributes

Here 2D cross-plot analysis is used to illuminate the variation of the azimuth (as the angle with respect to the north of a signal), the dip (respect to the 3D north coordinate reference system) versus the coherency attribute mapped out of the seismic dataset (Fig. 10b and Fig. 11a, c). Semblance and/or coherency values of the seismic can be extracted from any coherency volume attributes, while the reflector azimuth coordinate can be extracted from any azimuth volume (calculated as a time invariant volume). Many commercial interpretation software platforms return these volume attributes as matrices of data that can be further manipulated through numerical software packages (e.g. Matlab, Mathematica or Mathcad).

### 6.2. Cross-plot azimuth versus semblance: splitting signal from noise

To explore the potentiality of the method proposed we selected the seismic dataset from the Taranaki basin imaging the Parihaka normal fault (Fig. 5). Due to the high quality of the seismic dataset, the complexity of the fault and its related damage structures have been very well preserved and therefore represent an ideal seismic dataset where to explore image workflow processing. Azimuth and

semblance attributes from the Parihaka seismic dataset are cross-plotted (Fig. 10). The distribution clusters into a series of sub-populations that define particular preferred orientations (Fig. 10a). The tightest distribution represents the cluster of data with the lowest coherency values in the full dataset ( $45^\circ$  respect to North). These are distributed along a narrow range of azimuths (cluster 1). Two other clusters (volumes 2' and 3' in Fig. 10b) are identified, with wider azimuthal ranges (0–60 and 70–90). Data within these clusters can then be visualized back within the original seismic dataset. The tight azimuthal cluster corresponds to the Parihaka fault structure (see volume 1' in Fig. 10). The other two preferred azimuthal orientations 2' and 3' correspond to noisy and medium coherency zones surrounding the fault (Fig. 10) together with a NE-SW acquisition footprint noise. Thus this method demonstrates that the cross-plot method can be applied to track specific oriented noise or signal (e.g. the acquisition footprint), simply by selecting azimuth directions from within the volume. Note however, that it requires that the orientations of the fault systems do not coincide with that of the trajectory of the survey acquisition, as this would stack both sources of signal disruption.

### 6.3. Cross-plot dip versus semblance

A good quality seismic data example to test the method is the deep water Niger delta thrust belt (3D CGG see Fig. 5d) as it represent a very complex structural dataset where good details of the dip structures have been enhanced (see Higgins et al., 2007). Fig. 11(a–d) shows the application of our method to the 3D seismic volume from the deep water Niger delta. Here, two clear spikes

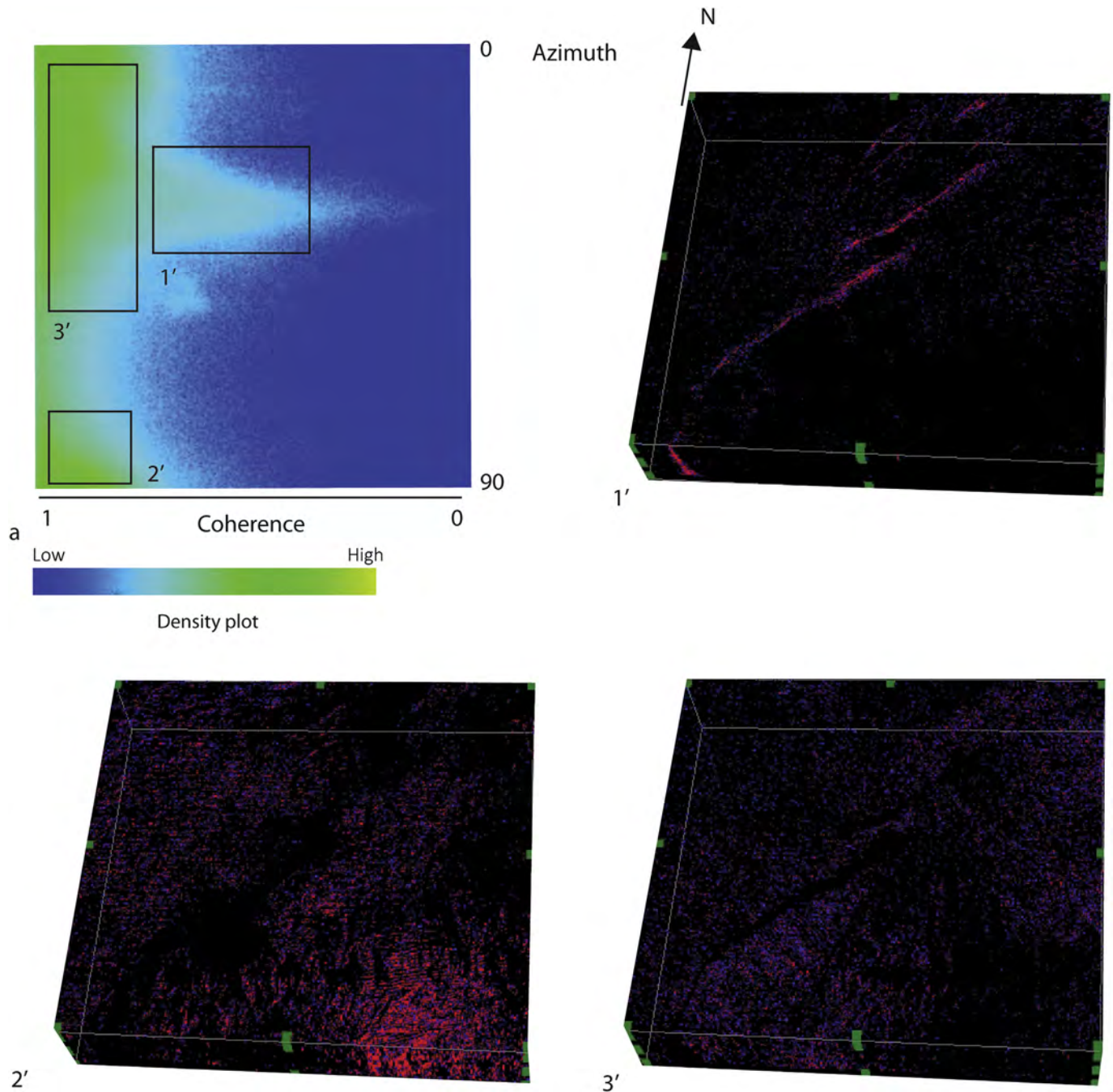


**Fig. 10.** a) cross-plot image of coherence versus azimuth, the squares 1', 2' and 3' represents selected cluster points to be visualize in the original dataset: sub -volume 1' expression of the cluster point in 1' (fault geobodies); sub-volume 2': expression of the cluster point in 2 (oriented acquisition noise); sub volume 3': expression of the cluster point in 3 (random noise).

(Fig. 11a, c) associated to the thrust-oriented features can be recognized along the dip axes in a time-coherency-dip cross-plotting volume. Once selected and visualized in the volume, the cross-plot maxima clearly correlates with the low semblance coherency zones associated with the major thrust zone (Fig. 11b, d) that show distinctive dip. Notice that the first spike is in reality a composite spike (black arrow in Fig. 11c) highlighting the more complex double nature of the thrust structures as shown in Fig. 11b.

Due to the similar along strike direction of the thrust structures the cross-plotting semblance coherence versus azimuth of those structures is not efficient in distinguishing the two structures

(Fig. 11e). The cross plot dip versus semblance is instead generally efficient for discriminating between zones of low coherence that are fault-related from those resulting from other sources of noise or signal disruption. Once selected, the subset of low-coherency data points can be plotted back and represented within a new visualization of the 3D seismic volume. This new seismic cube now highlights those SDZs associated with specific structures such as major faults without the interference of noise with oblique directions with respect to the structure of interest. This is a good starting point for further interpretation – relating the nature of the noise to the large scale faults.

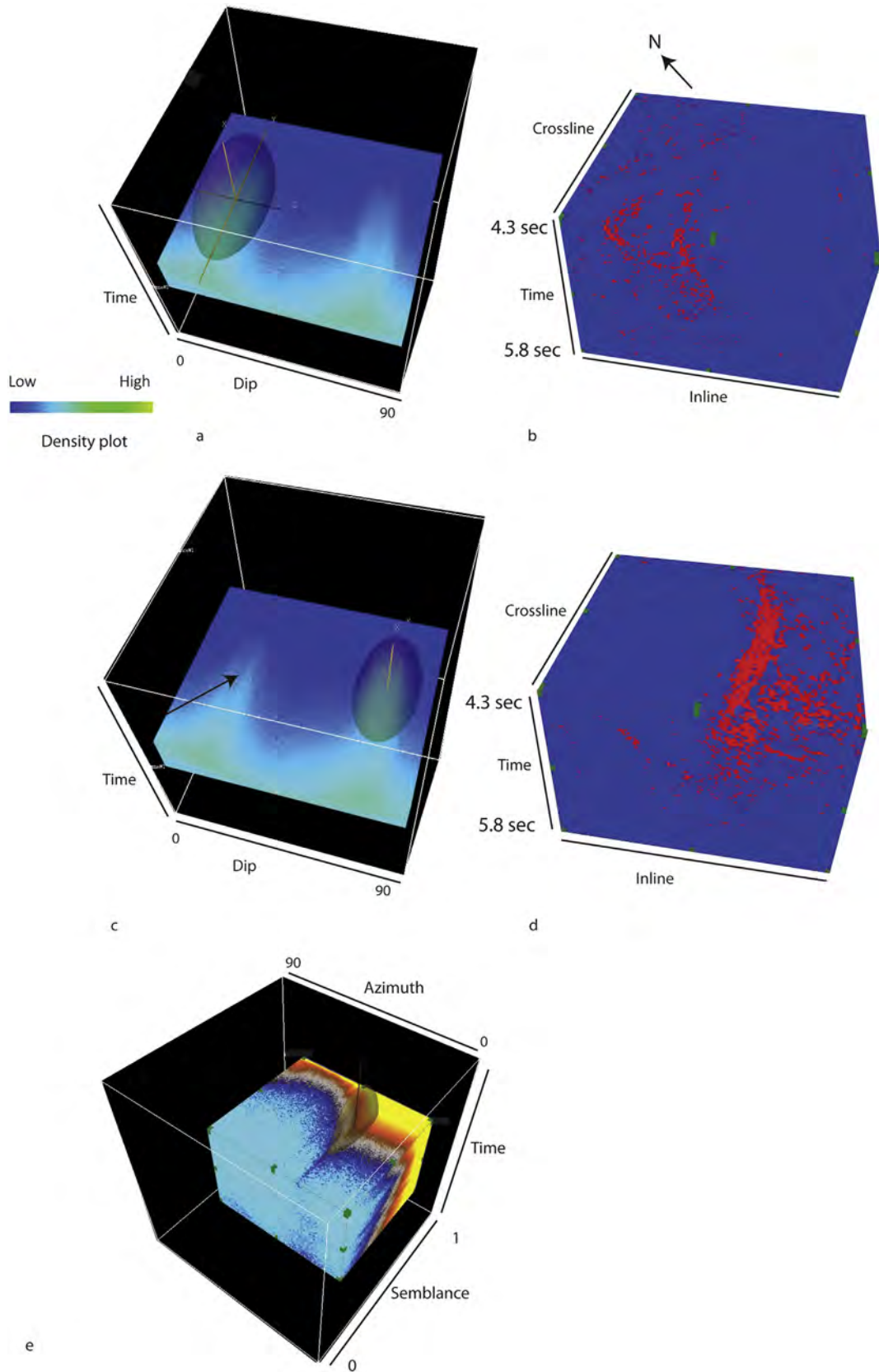


**Fig. 11.** Cross-plot cluster and image analysis of the semblance attributes of a shallow sub-volume imaging (in TWT ) the Deep water thrust belt from the Niger Delta. a) Dip versus semblance coherency cross-plot; b) visualization of the cluster in a; c) Dip versus semblance coherency cross-plot; d) visualization of the cluster point in d; e) azimuth versus semblance coherency crossplot view.

## 7. Mapping and characterizing the disturbance zones

Once the selection of the disturbance zones characterizing the main fault or deformation structure has been performed using the cross-plot across the area of interest, it is possible to proceed with the geobody characterization. Currently this can be achieved using either manual interpretation methods or automated techniques such as volumetric threshold-based extraction, or auto-tracking methods from a seed-point with threshold limit or range. Both methods have their flaws: manual interpretation of complex geological objects may be unrepeatable and time consuming, whilst automated methods rely on a consistent seismic expression within the object to be extracted and depend on the colour-imaging capabilities. It is not the scope of this paper to investigate the various techniques. Rather we present results from an existing approach (Paton et al., 2012) that adapts local data statistics to changes in seismic expression through a data volume. This approach combines manual interactive 3D editing of the geobodies with opacity threshold in areas where data-driven techniques alone are not sufficient to resolve the geological target. For our case studies we have extracted disturbance geobodies obtained using the cross-plot analysis of semblance versus azimuth attributes. Some noise with similar orientation to the SDZ is still resistant to the main cross-plot selection. The main outcomes are shown in Fig. 12. The SDZs tracked using the distributions of low semblance values have been rendered and extracted as single geobodies. These represent volumetric visualizations of the SDZs that have been pre-defined with low coherency thresholds (based on colour opacity values). The resultant geobodies can then be draped or filled with the correspondent original seismic signal properties or other attribute properties. It is these visualizations that underpin further analysis of the seismic texture. Fig. 13a represents slices through these geobodies.

### 7.1. Characterization of the disturbance zones using multi-attributes

Seismic signal properties were selected and extracted as SDZ geobodies using multi-attributes. This approach to investigate internal properties of the SDZ is similar to what used in seismic facies analysis (Dumay and Fournier, 1988; Posamentier and Kolla, 2003) where using the appropriate combination of seismic attributes for stratal units can predict lateral changes in geological properties

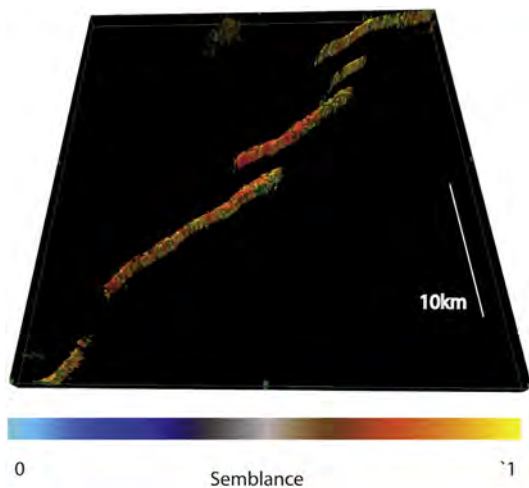


Fig. 12. 3D visualization as geobodies of the selected SDZ (same from diagram 1' in Fig. 11) using tensor attributes. The color bar refers to relative values of the semblance attributes draped on the tensor SDZ geobodies.

when calibrated with well information. When the geological information through a well log or field data is incomplete or non-existent, seismic facies analysis is called *unsupervised* (Fournier and Derain, 1995; Matos et al., 2007, 2011). In these cases the facies analysis is performed through the use of clustering algorithms. Without well log information, a mapped signal property cannot be strictly linked to specific petrophysical characteristics of the disturbance zone. This is a principal source of interpretation uncertainty. As well-log information is not available for our study, the interpretations of structural damage we draw from our visualizations are similarly uncertain.

#### 7.1.1. Multi attribute across the Parihaka SDZ

The first step of the workflow extracts the geobody using the tensor attribute (Fig. 12). This is readily achieved through the colour opacity by selecting the colour associated to the lowest tensor values. This surface represents the external skin of a minimum body volume of the SDZ (Fig. 12). The enclosed geobody is then populated with attributes extracted from the SDZ. The approach is illustrated in a sub-cropped volume of the Parihaka seismic dataset (Fig. 12) corresponding to a window centered on the horizons located between 0.850 and 0.950 ms. The sub volume was chosen because it addresses a series of horizons just below the seabed where the resolution is still very good (around 70 Hz mean frequency). Calculation of the multi-attributes values and re-population of the fault-related SDZ with these multi-attributes was then performed over the full area of the fault-related SDZ. In Fig. 13 the multi attribute analysis uses two amplitude-related attributes (envelope and standard deviation) together with the SO semblance coherency. In order to characterize their interplay, the attributes mapped into the geobody are then cross-plotted. The resultant cross-plot diagrams (Fig. 13b–d) are calculated from the data contained in a small sub volume (black box in Fig. 13a). This area is magnified and analyzed in Fig. 14 below.

#### 7.1.2. Cross-plotting amplitude and semblance properties

By cluster analysis, the cross-plot function between two or more attributes may be used to define different seismic facies. Here three attributes are compared: amplitude properties as the envelope; standard deviation; and SO semblance. The standard deviation is a multi-trace attribute calculated from values over a defined 3D neighbourhood. It can calculate sites of rapid change or variation in amplitude and highlight volumes of chaotic structure. The envelope (root of the square amplitude) is commonly linked to relative acoustic impedance and in some specific geological environments to lithology properties (proportional to the acoustic impedance, Chopra and Marfurt, 2005). Fig. 13b shows standard deviation values cross-plotted against envelope for the selected areas (Fig. 13a). The cross-plot displays a positive correlation between the envelope and standard deviation. This means that value of amplitude variability is proportional to the brightness within the SDZ. Portions of the SDZs where the amplitude signal is stable (low variability) are associated with low envelope values. In contrast, standard deviation and semblance show poor correlation (Fig. 13c) and are not considered further here. A negative correlation exists for the envelope versus semblance (Fig. 13d) and this is confirmed if we select the entire geobody area (Fig. 13e). Consequently low coherency portions appear statistically linked with high envelope. Therefore we use two relationships for further discussion – those between envelope and standard deviation together with semblance and envelope.

## 8. Results: construction of the facies framework

Fig. 14a is a blended map of semblance and envelope attributes

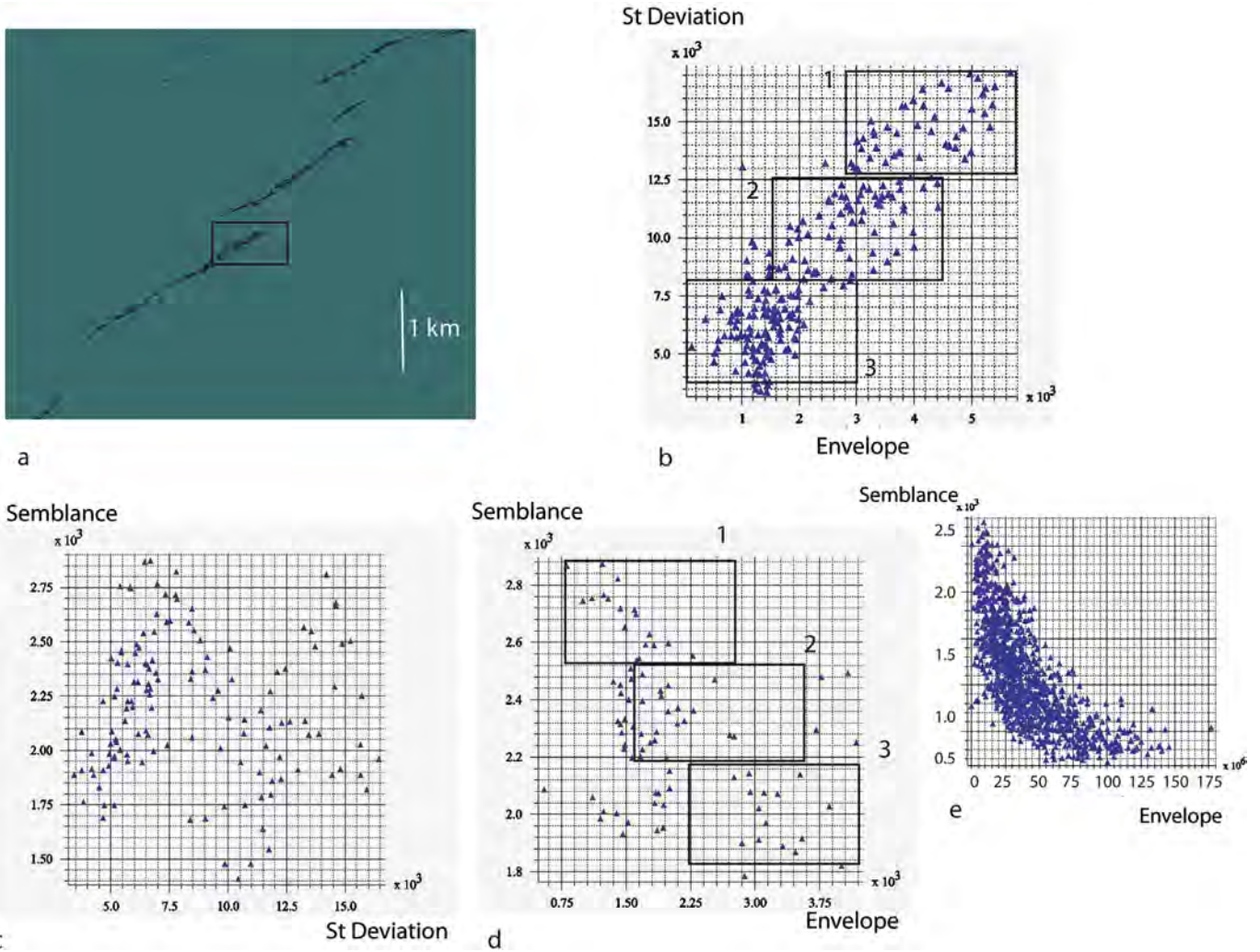


**Fig. 13.** a) Time slice at 900 ms (TWT) extracted from Fig. 12. b) Envelope versus St deviation crossplot. Numbered black squares represent the data point of the facies units; c) St deviation versus Semblance crossplot; d) Envelope versus Semblance. Numbered black square represent the data point of the facies units. e) envelope versus semblance crossplot of the full SDZ geobodies volume. See text for explanation.

for the selected area in the geobody, created by draping the semblance and envelope volumes (see appendix for a detailed description of the main workflow). High semblance and low values of envelope are represented in the blend volume by blue, while low semblance (or high incoherency) and high envelope is represented in red (Fig. 14a). Fig. 14c is the blended map of the standard deviation and envelope attributes volume draped into the selected geobody. Low values of standard deviation and low envelope are pale blue/white while wide values (high variability) and high envelope (brightness) are in red. These volume attributes were then used to create two facies maps using the statistical approach defined above by specific acceptance level: respectively a semblance/envelope facies (Fig. 14b) and the standard deviation/semblance facies (Fig. 14d). The significance of the facies from a specific selected area (shown on Fig. 14b, d) is represented by the numbered rectangle in the cross-plot diagram (Fig. 13b, d). A comparison between the blend maps and the facies provide a good basis for structural interpretation.

**8.1. Envelope/semblance facies map**

The following three main facies can be recognized (see small

colour legend Figs. 14b and 14d):

- 1-1- High envelope/high incoherency zones corresponding to zones where the signal has been strongly perturbed and the amplitude damaged (intense red facies 1-1, rectangle 1 in Fig. 13d)
- 1-2 - Intermediate coherency/amplitude (orange facies 1-2, rectangle 2 in Fig. 13d).
- 1-3 - Relative low amplitude/low incoherency represent zones where the signal is well defined and with relative low amplitude (pale red facies 1–3, rectangle 3 in Fig. 13d)

A comparison between Fig. 14a, b shows that the intense red colour of the facies 1-1 corresponds to the intense red colour of the blend map 1 (as indicated by the white arrows in Fig. 14b). Similar relationships apply to the other colours in sequence (white colour 2 in the blend map approximately matching with the pale facies 1–3, the blue with the facies 1–2).

**8.2. Envelope/standard deviation facies map**

Again three main facies (1-1; 1–2; 1–3 in Figs. 14b and d) can be recognized and broadly matched with the blend map (intense blue; white; red, Fig. 13c):

- 1-1- Facies of high variability/high envelope values (intense blue



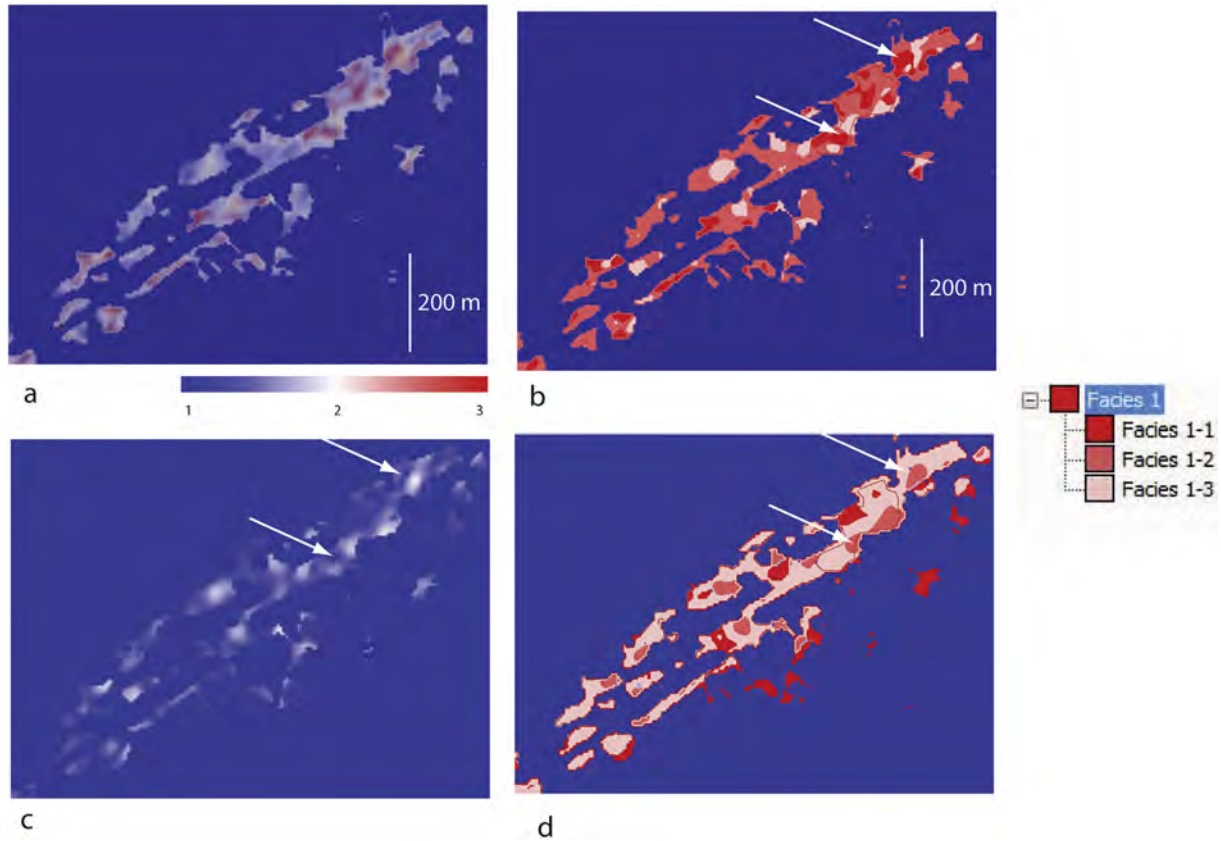


**Fig. 14.** Facies reconstruction within a selected area of the SDZ geobodies: a) blend map using semblance and envelope volume (1, 2 and 3 blend end member). b) Facies representing the cluster classification in 13d; c) blend map using Standard deviation and envelope data (colour expressed as in 14 a). d) Facies map representing the cluster classification in 13b. See text for explanation.

– facies 1-1; Rectangle 1, Fig. 13b)

1 -2- Intermediate coherency/amplitude (white - facies 1-2; Rectangle 2, Fig. 13b)

1-3- Facies of low envelope values/low variability that correspond to zones where the signal shows neither strong amplitude nor amplitude variation (red - facies 1-3; Rectangle 3, Fig. 13b)

If we compare Fig. 14b with Fig. 14d we can observe (as pointed by the white arrows) that the facies 1-1 associated with high incoherency and high envelope (see Fig. 14b) broadly corresponds with the red/pale facies with medium/brighter envelope and intermediate/high standard deviation (high incoherency imply high amplitude variability)). Again the facies characterized by low envelope and high stability (low variability) values broadly matches with the zone of high coherency (named facies 1-3 in Fig. 14b, d). The width and uncertainty of the limits are due by the complexity of the signal and the statistical threshold used to construct the two facies from the combined volumes.

The result is that it is possible to map amplitude related and semblance-related attributes and use those values to obtain facies of the signal response across the full FSDZ geobody (Fig. 12). Collectively they show patterns of differing signal properties across the SDZ.

## 9. Discussion

### 9.1. Interpreting the SDZ semblance-envelope based texture map

An integrated view of the mapped geobodies and the seismic reflectivity for the Parihaka fault is represented in Fig. 15. The

geobodies built from the seismic texture obtained using the envelope and SO semblance (Fig. 13b) are now visualized (using the same red facies colour 1 to 3 of Fig. 14) and tied by arbitrary lines imaging the envelope and the related reflectivity properties. The seismic color bar represents high envelope values in red (strong reflectivity) and low envelope values in blue. Strong red facies (facies 1-3) correspond to the reflectors characterized by medium/high envelope values coincident with area of strong reflector deflection (characterized by low coherency). Across the seismic line the red facies consistently match the medium and high envelope

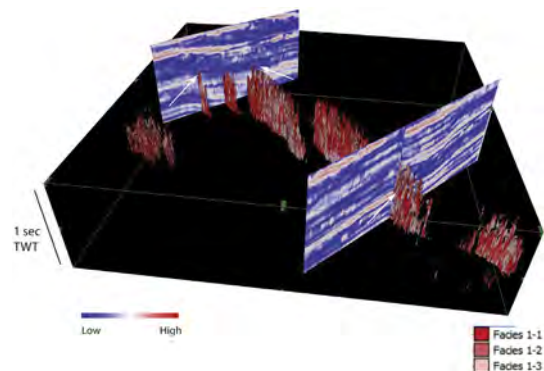


**Fig. 15.** Cross-section representation of two arbitrary seismic lines (expressed as envelope values) tying the Parihaka SDZ. The SDZ represents the entire fault analyzed and is expressed as geobodies facies map (using the envelope and semblance cross-plot classification values, Fig. 13d).

values associated with areas of strong incoherency. This facies is clearly sensitive to zones where the signal matches strong deformation and amplitude variation and support the facies distribution reconstructed through the seismic attributes. It suggests that there are promising indications that the SDZ can statistically store real signal responses and do not represent noise artefacts. A similar result has been recently proposed by Botter et al. (2014) through forward seismic imaging experiments using a 3D post stack dip migration simulator (Lecomte et al., 2015). Although the effect of coherent noise and the response of the coherency has not been taken into account in these experiment, their results emphasize that the character of SDZ is partly due to the seismic response of the damage and fault zone cores. Moreover Botter et al. (2014) RMS amplitude analysis across the fault discontinuity suggests that SDZs are directly correlated to changes in acoustic properties, especially at high wave frequencies. This seems to support the idea that despite the systematic effects of array acquisition parameters, the amplitude response within the SDZ could be related to change of the acoustic properties of the fault. Similarly, the clear correlation between amplitude response of the signal (envelope) and the coherency of the signal within the SDZs demonstrated by our study suggests that relationships between seismic waveform properties and the petrophysical response of large scale deformed structure should be investigated further.

### 9.2. Possible pitfalls in the calculation of attributes

As recently highlighted (e.g. Marfurt and Alves, 2015), an indiscriminate or automated use of seismic attributes, especially using dip or curvature (Chopra et al., 2011) without a detailed pre conditioning of the data (Chopra and Marfurt, 2007) commonly creates artefacts. These include apparent discontinuities or false fractures (known as “structural leakage”) or may be affected by acquisition footprint, migration operator aliasing, aliased shallow diffractions, and multiples. Low reflectivity may simply fall below the ambient noise level (Marfurt and Alves, 2015). Here, our procedure requires a pre-recognition of the main large-scale structure [(through edge preserving structural oriented filter or the analysis of steering dip and azimuth volumes using different sampling windows) together with matching the observation with conventional mapping across seismic sections. The use of cross-plot techniques to reduce the footprint noise or extract the structure of interest from the underpinning sedimentary structures of no interest for our analysis were key to reduce both the number of artefacts and the interference between signals of different geological origin. Our full analysis has been performed across quite a shallow portion of the data sub-volume that retains high frequencies (10–70 Hz), deep enough to be only partly affected from the main footprint acquisition (in any case reduced through the cross-plot analysis between coherency and azimuth) and in an area devoid of diffuse deformation and stratigraphic complexity. However, as indicated in Fig. 10, the cursory analysis of any 0 – 90 degree-oriented feature through the cross-plot analysis of the coherency versus azimuth allowed us to map not only different types of noise but also sedimentary features which are not of direct interest here.

### 9.3. Geological significance of SDZ

The two distinctive tectonic areas investigated here, demonstrate three end-members of possible structural deformation visible at seismic scale. The first represents an intense inverse thrust structure, the second the seismic expression of a fold, the third a normal fault zones surrounded by a wide spread area of strong fracture/secondary fault damage. The observed SDZ affecting

the forelimb of the fold structure is comparable to the fault-related SDZ (Fig. 4a, c). In both cases the two large structures are affected by signal disturbance where the amplitude, phase and coherency of the reflectors appear damaged. In the normal fault structure (Fig. 6a,b) the fine scale texture of the signal indicates that an intense vertical discontinuity is producing a wipe out zone with broader disturbance. As suggested elsewhere (Dutzer et al., 2009; Iacopini and Butler, 2011) and discussed below, these types of SDZ are repeatedly observed in submarine data and represent an unavoidable aspect of the deformation to deal with for reservoir modelling, restoration and balancing purposes. Within our thrust structure (Fig. 3a, b), the origin of small to sub-seismic scale features are less clearly interpreted in terms of inherent deformation structures. They may however be easily extracted, distinguished, mapped out, treating the disturbance zones as geobodies distributed across the boundary walls.

At outcrop scale, a damage zone is defined as the network of subsidiary features bounding the fault core zones (Caine et al., 1996; Hesthammer et al., 2000). However fault core show thickness of the order few mm to various meters while fault damage zones show thickness that usually span from cm scale to 100 m scale (Caine et al., 1996; Faulkner et al., 2010). Both objects are often at or below the limit of the seismic resolvability. The various SDZs analyzed here are significantly thicker than any equivalent damage or deformation structure observed in the field (Faulkner et al., 2010; Rotevatn and Fossen, 2011). This may caution against applying definitions or simplistic interpretations based on simple self-similarity through scale.

## 10. Conclusion

The study here represents a step forward in the seismic characterization of the fault structure and its surrounding noise through the use of seismic image processing methods. It represents part of on-going work aimed at recognizing seismic signatures related to distributed deformation (see Hesthammer et al., 2001; Botter et al., 2014; Marfurt and Alves, 2015). We demonstrate that, through seismic image processing and the use of cross-plot functions, it is possible to extract SDZs, to treat them as geobodies and explore their internal seismic texture. The following methods are proposed:

- An image processing workflow procedure to extract the structure oriented signal from the seismic footprint.
- A seismic image processing workflow to map the signal properties within the fault SDZ and reconstruct unsupervised seismic facies by using cluster analysis methods.

Further work is needed to apply the methodology across different fault damage zones through the inclusion of well log core information and by using seismicforward modelling tests to investigate if the seismic texture observed can be robustly linked to the petrophysics response (using inverse methods) of the fabric properties imaged within the fault SDZs.

## Acknowledgments

The seismic interpretation and image processing has been run in the SeisLab facility at the University of Aberdeen (sponsored by BG, BP and Chevron) Seismic imaging analysis was performed in Geoteric (ffA), and Mathematica (Wolfram research). Interpretation of seismic amplitudes was performed Petrel 2014 (Schlumberger). We thank Gaynor Paton (Geoteric) for in depth discussion on the facies analysis methodology and significant suggestions to improve the current paper. We thank the New Zealand government (Petroleum and Minerals ministry) and CGG for sharing the seismic dataset

utilized in this research paper. Seismic images used here are available through the Virtual Seismic Atlas ([www.seismicatlas.org](http://www.seismicatlas.org)). Nestor Cardozo and an anonymous reviewer are thanked for their constructive comments and suggestions that strongly improved the quality and organization of this paper.

## Appendix A. Supplementary data

Supplementary data related to this article can be found at <http://dx.doi.org/10.1016/j.jsg.2016.05.005>

## References

- Acharya, I., Ray, A.K., 2005. *Image Processing: Principles and Applications*. Wiley, p. 452.
- Berkhout, A.J., 1984. *Seismic Exploration-seismic Resolution: a Quantitative Analysis of Resolving Power of Acoustical Echo Techniques*. Geophysical Press, London.
- Biondi, B., 2006. 3D seismic imaging. *SEG. Investig. Geophys.* 14.
- Botter, C., Cardozo, N., Hardy, S., Leconte, I., Escalona, 2014. From mechanical modeling to seismic imaging of faults: a synthetic workflow to study the impact of faults on seismic. *Mar. Pet. Geol.* 57, 187–207.
- Boyer, S.J., Elliott, D., 1982. Thrust systems. *Bull. Am. Assoc. Pet. Geol.* 66, 1196–1230.
- Brown, A., 1996. *Interpretation of Three-dimensional Seismic Data*, seventh ed.
- Butler, R.H.W., McCaffrey, W.D., 2004. Nature of the thrust zones in deep water sand-shale sequences: outcrop examples from the Champsaur sandstones of SE France. *Mar. Pet. Geol.* 21, 911–921.
- Butler, R.W.H., Paton, D.A., 2010. Evaluating lateral compaction in deepwater fold and thrust belts: how much are we missing from Nature's Sandbox? *GSA Today* 20, 4–10.
- Butler, R.W.H., 1987. Thrust sequences. *J. Geol. Soc.* 144, 619–634.
- Caine, J.S., Evans, J.P., Forster, C.B., 1996. Fault zone architecture and permeability structure. *Geology* 24, 1025–1028.
- Cardozo, N., Bhalla, K., Zehnder, A.T., Allmendinger, R.W., 2003. Mechanical models of fault propagation folds and comparison to the trishear kinematic model. *J. Struct. Geol.* 25, 1–18.
- Cartwright, J.A., Trudgill, B.D., Mansfield, C.S., 1995. Fault growth by segment linkage: an explanation for scatter in maximum displacement and trace length data from the Canyonlands Grabens of SE Utah. *J. Struct. Geol.* 17, 1319–1326.
- Childs, C., Nicol, A., Walsh, J.J., Watterson, J., 1996. Growth of vertically segmented normal faults. *J. Struct. Geol.* 18, 1389–1397.
- Childs, C., Nicol, A., Walsh, J.J., Watterson, J., 2003. The growth and propagation of syn sedimentary faults. *J. Struct. Geol.* 25, 633–648.
- Chopra, S., Marfurt, K.J., 2005. Seismic Attributes – a historical perspective. *Geophysics* 70, 3–28.
- Chopra, S., Marfurt, K.J., 2007. Curvature attribute applications to 3D seismic data. *Lead. Edge* 26 (4), 404–414.
- Chopra, Marfurt, K.J., 2010. Integration of coherence and volumetric curvatures images. *Lead. Edge* 30, 1092–1106.
- Chopra, S., Misra, S., Marfurt, K., 2011. Coherence and curvature attributes on pre-conditioned seismic dataset. *Lead. Edge* 32, 260–266.
- Cohen, I., Coult, N., Vassiliou, A., 2006. Detection and extraction of fault surfaces in 3D seismic data. *Geophysics* 71, 21–27.
- Corradi, a., Ruffo, P., Visentin, C., 2009. 3D hydrocarbon migration by percolation technique in an alternate sand–shale environment described by a seismic facies classified volume. *Mar. Pet. Geol.* 26, 495–503.
- Cowie, P.A., Scholz, C.H., 1992. Displacement-length scaling relationship for faults: data synthesis and discussion. *J. Struct. Geol.* 14, 1149–1156.
- Dorn, G.A., 1998. Modern 3-D seismic interpretation. *The Leading Edge* 17 (9). <http://dx.doi.org/10.1190/1.143.1262-1262>.
- Dumay, J., Fournier, F., 1988. Multivariate statistical analyses applied to seismic facies recognition. *Geophysics* 53, 1151–1159.
- Dutser, J.F., Basford, H., Purves, S., 2009. Investigating fault sealing potential through fault relative seismic volume analysis. *Pet. Geol. Conf. Ser.* 7, 509–515. <http://dx.doi.org/10.1144/0070509>.
- Evans, D.J., Meneilly, A., Brown, G., 1992. Seismic facies analysis of Westphalian sequences of the southern North Sea. *Mar. Pet. Geol.* 9, 578–589.
- Fagin, 1996. The fault shadow problem: its nature and elimination. *Lead. Edge* 15, 1005–1013.
- Faulkner, D.R., Jackson, C.A.L., Lunn, R., Schlisch, R., Shipton, Z., Wibberley, C., Withjack, M., 2010. A review of recent developments regarding the structure, mechanics and fluid flow properties of fault zones. *J. Struct. Geol.* 32, 1557–1575.
- Fehmers, G., Höcker, C., 2003. Fast structural interpretation with structure-oriented filtering. *Geophysics* 68, 1286–1293. <http://dx.doi.org/10.1190/1.1598121>.
- Fournier, F., Derain, J.F., 1995. A statistical methodology for deriving reservoir properties from seismic data. *Geophysics* 60, 1437–1450.
- Gao, D., 2003. Volume texture extraction for 3D seismic visualization and interpretation. *Geophysics* 68, 1294–1302.
- Gao, D., 2007. Application of three-dimensional seismic texture analysis with special reference to deep-marine facies discrimination and interpretation: offshore Angola, West Africa. *AAPG Bull.* 91, 1665–1683.
- Gelius, L.J., Asgedom, E., 2011. Diffraction – limited imaging and beyond-the concept of super resolution. *Geophys. Prospect.* 59, 400–421.
- Gerard, J., Buhrig, C., 1990. Seismic facies of the Permian section of the Barents Shelf: analysis and interpretation. *Mar. Pet. Geol.* 7, 234–252.
- Gersztenkorn, G., Marfurt, K.J., 1999. Eigenstructure-based coherence computations as an aid to 3-D structural and stratigraphic mapping. *Geophysics* 64, 1468–1479.
- Giba, M., Nicol, A., Walsh, J.J., 2010. Evolution of faulting and volcanism in a Back-Arc Basin and its implications for subduction processes. *Tectonic* 29, TC4020.
- Giba, M., Walsh, J.J., Nicol, A., 2012. Segmentation and growth of an obliquely reactivated normal fault. *J. Struct. Geol.* 39, 253–267.
- Hale, D., 2013. Methods to compute fault images, extract fault surfaces and estimate fault throws from 3D seismic images. *Geophysics* 78, 33–43.
- Haralick, R.M., Shanmugam, K., Dinstein, I., 1973. Textural features for image classification. *IEEE Trans. Syst. Man Cybern.* 3, 610–621.
- Hardy, S., Allmendinger, R., 2011. Trishear. A review of kinematics, mechanics, and 783 applications. In: McClay, K., Shaaw, J., Suppe, J. (Eds.), *Thrust Fault-related Folding*, vol. 94. American Association of Petroleum Geologists Memoir, pp. 95–119.
- Henderson, J., Purves, S., Leppard, C., 2007. Automated delineation of geological elements from 3D seismic data through analysis of multi-channel, volumetric spectral decomposition data. *First Break* 25, 87–93.
- Henderson, J., Purves, S., Fisher, G., Leppard, C., 2008. Delineation of geological elements from RGB color blending of seismic attribute volume. *Lead. Edge* 8, 342–349.
- Hesthammer, J., Johansen, T.E.S., Watts, L., 2000. Spatial relationships within fault damage zones in sandstone. *Mar. Pet. Geol.* 17, 873–893.
- Hesthammer, J., Landrø, M., Fossen, H., 2001. Use and abuse of seismic data in reservoir characterisation. *Mar. Pet. Geol.* 18, 635–655.
- Higgins, S., Davies, R.J., Clarke, B., 2007. Antithetic fault linkages in a deep water fold and thrust belt. *J. Struct. Geol.* 29, 1900–1914.
- Higgins, S., Clarke, B., Davies, R.J., Cartwright, J., 2009. Internal geometry and growth history of a thrust-related anticline in a deep water fold belt. *J. Struct. Geol.* 31, 1597–1611.
- Hu, Z., Huang, J.B., Yang, M.H., 2010. Single Image deblurring with adaptive dictionary learning. In: *IEEE international conference on image processing*. China, Hong Kong, pp. 1169–1172.
- Iacopini, D., Butler, R.W.H., 2011. Imaging deformation in submarine thrust belts using seismic attributes. *Earth Planet. Sci. Lett.* 302, 414–422.
- Iacopini, D., Butler, R.W.H., Purves, S., 2012. Seismic imaging of thrust faults and structural damage: a visualization workflow for deepwater thrust belts. *First Break* 30, 39–46.
- Jamieson, W.J., 2011. Geometrical analysis of fold development in overthrust terrane. *J. Struct. Geol.* 9, 207–219.
- Jones, G., Knipe, R.J., 1996. Seismic attribute maps; application to structural interpretation and fault seal analysis in the North Sea Basin. *First Break* 14, 10–12.
- Khaidukov, V., Landa, E., Moser, T.J., 2004. Diffraction imaging by focusing – defocusing: an outlook on seismic superresolution. *Geophysics* 69, 1478–1490.
- Lecomte, I., Lavadera, P.L., Anell, I.M., Buckley, S.J., Heeremans, M., 2015. Ray-based seismic modeling of geologic models: understanding and analyzing seismic images efficiently. *Interpretation* 3 (4). <http://dx.doi.org/10.1190/INT-2015-0061.1>.
- Long, J.J., Imber, J., 2010. Geometrically coherent continuous deformation in the volume surrounding a seismically imaged normal fault-array. *J. Struct. Geol.* 32, 222–234.
- Love, P.L., Simaan, M., 1984. Segmentation of stacked seismic data by the classification of image texture. In: *54th Annual International Meeting, SEG*, pp. 480–482. Expanded Abstracts.
- Marfurt, K.J., Alves, T.M., 2015. Pitfalls and limitations in seismic attribute interpretation of tectonic features. *Interpretation* 3, 5–15. <http://dx.doi.org/10.1190/INT-2014-0122.1>.
- Marfurt, K.J., Chopra, S., 2007. *Seismic Attributes for Prospect Identification and Reservoir Characterization*. SEG Geophysical development (11).
- Matos, de M.C., Osorio, P.L.M., Johann, P.R.S., 2007. Unsupervised seismic facies analysis using wavelet transform and self-organizing maps. *Geophysics* 72, 9–21.
- Matos, M.C., Yenugu, M., Angelo, S.M., Marfurt, K.J., 2011. Integrated seismic texture segmentation and cluster analysis applied to channel delineation and chert reservoir characterization. *Geophysics* 76, 11–21.
- McArdle, N.J., Iacopini, D., KunleDare, M.A., Paton, G.S., 2014. The use of geologic expression workflows for basin scale reconnaissance: a case study from the Exmouth Subbasin, North Carnarvon Basin, northwestern Australia. *Interpretation* 2, 163–177.
- Mitra, S., 1990. Faults propagation fold: geometry, kinematic evolution, traps. *Am. Assoc. Pet. Geol. Bull.* 74, 921–945.
- Morgan, R., 2003. Prospectivity in ultradeep water: the case for petroleum generation and migration within the outer parts of the Niger Delta apron. In: Arthur, T.J., MacGregor, D.S., Cameron, N.R. (Eds.), *Petroleum Geology of Africa: New Themes and Developing Technologies*, Special. Publication. Geological Society of London, vol. 207, pp. 151–164.
- Moser, T.J., Howard, C.B., 2008. Diffraction imaging in depth. *Geophys. Prospect.* 56, 627–641.
- Neidell, N.S., Taner, M.T., 1971. Semblance and other coherency measures for

- multichannel data. *Geophys.* 36, 482–497.
- Partyka, G.A., Gridley, J.M., Lopez, J., 1999. Interpretational applications of spectral decomposition in reservoir characterization. *Lead. Edge* 18, 353–360.
- Paton, G., Elghorori, A., McArdle, N., 2012. Adaptive Geobodies: Extraction of Complex Geobodies from Multi-attribute Data Using a New Adaptive Technique. AAPG Search and Discovery Article #90141©2012, GEO-2012.
- Posamentier, H., Kolla, V., 2003. Seismic geomorphology and stratigraphy of depositional elements in deep-water settings. *J. Sediment. Res.* 73, 367–388.
- Purves, S., 2014. Phase and Hilbert transform. *Lead. Edge* 34, 1246–1253.
- Rotevatn, A., Fossen, H., 2011. H. Simulating the effect of subseismic fault tails and process zones in a siliciclastic reservoir analogue: implications for aquifer support and trap definition. *Mar. Pet. Geol.* 28, 1648–1662.
- Schlaf, J., Randen, T., Sonneland, 2004. Introduction to seismic texture. *Mathematical methods and modelling in hydrocarbon exploration and production*. *Math. Ind. Ser.* 7, 1–23.
- Suppe, J., Medwedeff, D.A., 1990. Geometry and kinematics of fault-propagation folding. *Eclogae Geologicae Helveticae* 83, 409–454.
- Suppe, J., 1983. Geometry and Kinematic of fault bend folding. *Am. J. Sci.* 283, 684–721.
- Taner, M.T., Koehler, F., Sheriff, R.E., 1979. Complex trace analysis. *Geophysics* 44, 1041–1063.
- Vermeer, G.J.O., 2009. 3D Seismic Survey Design. *Geophysical References Series*, pp. 17–67.
- Walsh, J., Watterson, J., Yielding, G., 1991. The importance of small-scale faulting in regional extension. *Nature* 351, 391–393.
- Walsh, J.J., Nicol, A., Childs, C., 2002. An alternative model for the growth of faults. *J. Struct. Geol.* 24, 1669–1675.
- Walsh, J.J., Bailey, W.R., Childs, C., Nicol, A., Bonson, C.G., 2003a. Formation of segmented normal faults: a 3-D perspective. *J. Struct. Geol.* 25, 1251–1262.
- Walsh, J.J., Childs, C., Imber, J., Manzocchi, T., Watterson, J., Nell, P.A.R., 2003b. Strain localisation and population changes during fault system growth within the Inner Mora Firth, Northern North Sea. *J. Struct. Geol.* 25, 307–315.
- West, B., May, S., Eastwood, J.E., Rossen, C., 2002. Interactive seismic facies classification using textural and neural networks. *Lead. Edge* 21, 1042–1049.
- Wibberley, C.A.J., Yielding, G., Di Toro, G., 2008. Recent advances in the understanding of fault zone internal structure; a review. In: Wibberley, C.A.J., Kurz, W., Imber, J., Holdsworth, R.E., Collettini, C. (Eds.), *Structure of Fault Zones: Implications for Mechanical and Fluid-flow Properties*, Geological Society of London Special Publication, vol. 299, pp. 5–33.
- Widess, M.B., 1973. How thin is a thin bed? *Geophysics* 38, 1176–1180.
- Zavalishin, B.R., 2000. Diffraction problems of 3D seismic imaging. *Geophys. Prospect.* 48, 631–645.
- Zhang, Y., Sun, J., 2009. Practical issues in reverse time migration true amplitude gathers, noise removal and harmonic source encoding. *First Break* 26, 134–156.